Published in final edited form as:

J Neurosci Res. 2021 August ; 99(8): 1922–1939. doi:10.1002/jnr.24683.

Chronic intermittent ethanol and lipopolysaccharide exposure differentially alter Iba1-derived microglia morphology in the prelimbic cortex and nucleus accumbens core of male Long-Evans rats

Benjamin M. Siemsen[1,2], **Justine D. Landin**[2], **Jon A. McFaddin**[1], **Kaylee N. Hooker**[1], **Lawrence J. Chandler**[2], **Michael D. Scofield**[1,2]

[1]Department of Anesthesiology and Perioperative Medicine, Medical University of South Carolina, Charleston, SC, USA

[2]Department of Neuroscience, Medical University of South Carolina, Charleston, SC, USA

Abstract

Accumulating evidence has linked pathological changes associated with chronic alcohol exposure to neuroimmune signaling mediated by microglia. Prior characterization of the microglial structure-function relationship demonstrates that alterations in activity states occur concomitantly with reorganization of cellular architecture. Accordingly, gaining a better understanding of microglial morphological changes associated with ethanol exposure will provide valuable insight into how neuroimmune signaling may contribute to ethanol-induced reshaping of neuronal function. Here we have used Iba1-staining combined with high-resolution confocal imaging and 3D reconstruction to examine microglial structure in the prelimbic (PL) cortex and nucleus accumbens (NAc) in male Long-Evans rats. Rats were either sacrificed at peak withdrawal following 15 days of exposure to chronic intermittent ethanol (CIE) or 24 hr after two consecutive injections of the immune activator lipopolysaccharide (LPS), each separated by 24 hr. LPS

Correspondence Benjamin M. Siemsen, Departments of Anesthesiology and Neuroscience, Medical University of South Carolina, 173 Ashley Avenue, Charleston, SC 29425, USA, siemsen@musc.edu.

Benjamin M. Siemsen and Justine D. Landin contributed equally and should be considered joint first authors in that order.

AUTHOR CONTRIBUTIONS

Investigation, B.M.S., J.D.L., J.A.M., and K.N.H.; *Writing – Reviewing, & Editing*, B.M.S., J.D.L., L.J.C., and M.D.S.; *Conceptualization*, B.M.S., L.J.C., and M.D.S.; *Methodology*, B.M.S. and M.D.S.; *Visualization*, B.M.S. and M.D.S.; *Supervision*, L.J.C. and M.D.S.

CONFLICT OF INTEREST

The authors declare that they have no conflict of interest.

DECLARATION OF TRANSPARENCY

The authors, reviewers and editors affirm that in accordance to the policies set by the *Journal of Neuroscience Research*, this manuscript presents an accurate and transparent account of the study being reported and that all critical details describing the methods and results are present.

PEER REVIEW

The peer review history for this article is available at https://publons.com/publon/10.1002/jnr.24683.

DATA AVAILABILITY STATEMENT

All morphological data for microglia filament analyses can be found at Neuromorpho: neuromorpho.org/dableFiles/siemsen/Supplementary/Siemsen_Scofield.zip.

Transparent Peer Review Report

Transparent Science Questionnaire for Authors

Edited by Alex Marshall. Reviewed by Adron Harris, Ryan P. Vetreno, and Justin McClain.

exposure resulted in dramatic structural reorganization of microglia in the PL cortex, including increased soma volume, overall cellular volume, and branching complexity. In comparison, CIE exposure was associated with a subtle increase in somatic volume and differential effects on microglia processes, which were largely absent in the NAc. These data reveal that microglial activation following a neuroimmune challenge with LPS or exposure to chronic alcohol exhibits distinct morphometric profiles and brain region-dependent specificity.

Keywords

chicken anti-GFP (RRID:AB_300798); chronic intermittent ethanol; goat anti-chicken; Alexa488 (RRID:AB_2636803); goat anti-rabbit; Alexa647 (RRID: AB_2722623); LPS; microglia; nucleus accumbens; prelimbic cortex; rabbit anti-Iba1 (RRID:AB_8939504)

1 | INTRODUCTION

Microglia participate in neuroimmune signaling induced by exposure to environmental insults by releasing cytokines and neuromodulators to support healthy central nervous system function and to regulate synaptic transmission (Czeh, Gressens, & Kaindl, 2011). However, dysfunctional cognitive processes that occur during aging, neurodegenerative disorders, and alcohol use disorder (AUD) have been linked to aberrant or dysfunctional activation of microglia in specific brain regions (Salter & Stevens, 2017; Sarlus & Heneka, 2017). AUDs in particular represent a significant public health concern that places an immense burden on both individuals and society (Kranzler & Soyka, 2018). Rodent models of chronic alcohol exposure, which reproduce the somatic symptoms of physical dependence and withdrawal observed in humans (Gilpin, Richardson, Cole, & Koob, 2008), also engage neuropathological processes that parallel what has been observed in brains from human alcoholics. Aside from the established link between alcohol-induced neuroplastic changes in neurotransmitter systems such as glutamate, GABA, and dopamine (for review see Tsai & Coyle, 1998), there is accumulating clinical (Beech et al., 2012; Devalaraja, Mcclain, Barve, Vaddi, & Hill, 1999; Manzardo, Poje, Penick, & Butler, 2016) and preclinical (Marshall et al., 2013; McClain, Hayes, Morris, & Nixon, 2011) evidence for the role of altered neuroimmune activity in the neuroadaptations induced by chronic ethanol exposure that may facilitate dysfunctional, frontal cortical-dependent, cognitive processes. As an example, immunoreactivity of ionized calcium-binding adaptor molecule 1 (Iba1), a protein specifically expressed in microglia (Ito, Imai, Ohsawa, Nakajima, Fukuuchi, & Kohsaka, 1998), is increased in postmortem brains of alcoholic patients (He & Crews, 2008).

Microglia express several membrane receptors that respond to molecular patterns associated with damage or pathogens, leading to an innate or adaptive immune response (Kigerl, de Rivero Vaccari, Dietrich, Popovich, & Keane, 2014). The superfamily of toll-like receptors (TLRs) are particularly important for recognizing extracellular signals linked to cellular damage and promoting the release of cytokines in response (Olson & Miller, 2004). Canonically, systemic injections of lipopolysaccharide (LPS) have been utilized to increase TLR4-dependent central microglia activation (Hines, Choi, Hines, Phillips, & MacVicar, 2013). Interestingly, several psychoactive compounds, such as opioids and cocaine, also

activate microglia by binding to and activating TLR4, leading to central immune signaling (Hutchinson et al., 2012; Northcutt et al., 2015). Akin to opioids and cocaine, studies have shown that ethanol exposure leads to microglia activation by increasing TLR4 and tumor necrosis factor alpha (TNFα) receptor-dependent neuroimmune signaling (Crews, Walter, Coleman, & Vetreno, 2017; Liu et al., 2011). Interestingly, ethanol exposure during adolescence increases TLR4 expression and increases the abundance of ligands for TLR4, including the damage-associated high-mobility group box 1 (Crews & Vetreno, 2016). However, the degree to which ethanol leads to TLR4-dependent neurotoxic insult is currently under debate (Alfonso-Loeches, Pascual-Lucas, Blanco, Sanchez-Vera, & Guerri, 2010; Bi et al., 2005; Cruz, Meireles, & Silva, 2017; Marshall et al., 2013). Nevertheless, knockout studies support a TLR4-based mechanism for ethanol's action on microglia, as loss of TLR4 prevents ethanol-induced microglial upregulation in the cortex and cytokine release in culture (Fernandez-Lizarbe, Pascual, & Guerri, 2009). Aside from TLR4, ethanol also acts directly on NADPH oxidase (Yang et al., 2014), inducing the release of reactive oxygen species from microglia, which have been linked to alcohol-induced neurodegeneration (Qin & Crews, 2012). Further, systemic administration of microglia activation inhibitor Minocycline has been shown to decrease ethanol self-administration (Agrawal, Hewetson, George, Syapin, & Bergeson, 2011). Collectively, these data support a role for microglia activation in the ethanol-induced neuroimmune and neuroinflammatory cascades linked to the disruption of cognitive processes mediating the maintenance of escalated ethanol drinking.

As Iba1 is specifically expressed in microglia in the CNS (Ahmed et al., 2007; Ito et al., 1998), traditional immunohistochemical labeling and detection of Iba1 has provided valuable insight into brain region-specific adaptations in microglia structure and proliferation following ethanol exposure. Several studies have shown that chronic ethanol exposure in rats increases the number of Iba1-positive cells, or increases Iba1 signal intensity, in a region-specific manner. For example, while 6 months of voluntary consumption of a 20% aqueous ethanol solution followed by 2 months of withdrawal did not alter the total number of microglia in the hippocampus, it did increase the proportion of activated microglia as indicated by elevated CD11b immunoreactivity (Cruz et al., 2017). Studies examining large numbers of microglia at relatively lowmagnification have reported that Iba1 intensity is increased in a TLR4-dependent manner within a number of brain regions, including the prefrontal cortex (PFC). This was observed following 35 days of chronic intermittent ethanol (CIE) exposure, which was diminished after 28 days of withdrawal (Sanchez-Alavez et al., 2019). As such, it is likely that ethanol-induced activation of microglia plays a role in the neuroadaptations associated with chronic alcohol exposure.

Microglia are exceptionally morphologically dynamic (Avignone, Lepleux, Angibaud, & Nägerl, 2015), with activation-associated alterations in soma size and branching patterns serving as structural biomarkers for neuroimmune activation (Davis, Salinas-Navarro, Cordeiro, Moons, & De Groef, 2017; Fernández-Arjona, Grondona, Granados-Durán, Fernández-Llebrez, & López-Ávalos, 2017; Morrison, Young, Qureshi, Rowe, & Lifshitz, 2017). Further, recent studies demonstrate brain region-specific heterogeneity in microglial morphology (Olah, Biber, Vinet, & Wgm Boddeke, 2011) and gene expression profiles

(Grabert et al., 2016), establishing brain region heterogeneity and supporting a clear link between microglia structure and function. Interestingly, even *within* brain regions individual microglia occupy a broad spectrum of activation states, and thus structural signatures (Harry & Kraft, 2012). Historically, microglia morphology has been used to classify microglia into either an activated or a resting state. However, a binary two-state categorization may be overly simplistic given that microglia constantly survey and respond to the surrounding microenvironment and likely respond by progressing through a continuum of differential activation states (Nimmerjahn, Kirchhoff, & Helmchen, 2005). Microglial processes are uniquely plastic and traverse the parenchyma at a rapid rate of 1–3 μm per minute (Nimmerjahn et al., 2005), influencing synaptic transmission as they sample the interstitial fluid and respond to stimuli with the release of neuromodulators (Kettenmann, Kirchhoff, & Verkhratsky, 2013).

The morphological signature of microglial cells tightly correlates with their functional states (Beynon & Walker, 2012; Karperien, Ahammer, & Jelinek, 2013; Morrison & Filosa, 2013). For instance, ramified microglia are characterized by thin and elongated processes and are canonically considered to be in a “resting” state. Environmental challenges that induce neural inflammation can transform microglia into an “ameboid” or “reactive” state, often characterized by an enlarged soma and thick or condensed processes. Once activated, microglia upregulate specific receptors and express secretory analogues that contribute to the defense of the central nervous system to environmental insults (Bohatschek, Kloss, Kalla, & Raivich, 2001). In general, microglia are remarkably sensitive to neural insult, and thus environmental challenges can produce rapid and extensive adaptations in microglial structure and function (Dubbelaar, Kracht, Eggen, & Boddeke, 2018).

Although a significant body of work exists regarding the impacts of ethanol on microglia and neuroimmune signaling (for review see Chastain & Sarkar, 2014), to date a systematic analysis of microglia morphological adaptations following CIE exposure has yet to be comprehensively conducted using high-resolution confocal microscopy and high fidelity digital reconstruction. Moreover, the effects of ethanol withdrawal have not been directly compared to canonical inducers of microglia activation, such as LPS. Here we show that CIE exposure of male rats produces brain region-dependent alterations in microglia morphometric features that display overlapping as well as dichotomous alterations induced by subchronic (2-day) immune activation following systemic LPS administration.

2 | MATERIALS AND METHODS

2.1 | Animal subjects

Male Long-Evans rats ($N = 15$) were obtained from Envigo (Indianapolis, IN). Upon arrival, rats were single housed in standard polycarbonate cages in a temperature-controlled vivarium and maintained on a 12-hr/12-hr reverse light/dark cycle (lights on at 21:00 hr) with *ad libitum* access to food and water throughout the experiment. Male *Cx3cr1*^{CreER}-Enhanced Yellow Fluorescent Protein (EYFP) transgenic mice ($N = 3$) were purchased from Jackson Laboratories (#021160). These mice constitutively express EYFP in lieu of endogenous Cx3cr1 brain-wide in microglia (Bult et al., 2018). All experiments were performed in accordance with guidelines for animal care established by the National

Institutes of Health and approved by MUSC's Institutional Animal Care and Use Committee. When appropriate, all animal subjects were randomly assigned to experimental groups.

2.2 | Chronic intermittent ethanol exposure

Chronic intermittent ethanol exposure was initiated using a well-characterized vapor inhalation model (Trantham-Davidson et al., 2014). In brief, adult male Long-Evans rats at postnatal day (PD) 90 ($n = 5$) were subjected to 15 consecutive days of intermittent ethanol vapor exposure. Each exposure day consisted of placing rats in standard housing cages into clear acrylic ethanol vapor exposure chambers (Plas-Labs; Lansing, MI) for a period of 14 hr/day. During the 10 hr out of the chambers, the rats were returned to the vivarium. Rats were placed into the chambers at 18:00 hr and removed at 08:00 hr. This CIE exposure paradigm was modeled after O'Dell, Roberts, Smith, and Koob (2004) and was chosen as it has been shown to enhance ethanol self-administration during withdrawal. Our laboratory has previously used this paradigm to show that prefrontal cortical-dependent cognitive flexibility, and associated dopamine-dependent prefrontal cortical excitatory transmission are disrupted during withdrawal from CIE (Trantham-Davidson et al., 2014). Immediately upon removal from the vapor chambers, a 5-point behavioral intoxication scale was utilized to assess the level of intoxication (Gass et al., 2014; Nixon & Crews, 2002). Also immediately prior to placing the rats back into the chambers following the 10-hr ethanol withdrawal period, the severity of withdrawal based upon somatic (posture/gait, tail stiffness, and ventromedial distal limb flexion) signs was assessed using a 6-point rating system (maximum score of 2 for each of the three somatic categories) (Nixon & Crews, 2002; Trantham-Davidson et al., 2014). On days 1, 5, 10, and 15, tail blood (40 μl) was collected immediately upon removal from chambers for subsequent determination of blood ethanol concentration (BEC). Air-exposed control rats ($n = 5$) were treated similar to the CIE-exposed rats except they were not placed into the ethanol vapor chambers, and served as the control group for all analyses.

2.3 | LPS injections

A subset of male Long-Evans rats ($n = 5$) received intraperitoneal injections of 1.0 mg/kg LPS from *Escherichia coli* (Sigma-Aldrich, L2630) in sterile saline (0.9%) once per day for two consecutive days. This paradigm was chosen in light of recent data indicating that the peak induction of brain cytokines (TNFα, IL-6, IL-1β), as well as microglial structural reorganization, occurs after two LPS (1 mg/kg) treatments, but sensitizes after additional injections. This treatment also induces mild sickness behavior and transient weight loss (Wendeln et al., 2018). Rats were then perfused 24 hr after the second injection of LPS.

2.4 | Immunohistochemistry

Mice or rats were heavily anesthetized with urethane (30% w/v) and then transcardially perfused with 120 ml (rats) or 20 ml (mice) of 0.1M phosphate-buffered saline (PBS)(pH 7.4) followed by 180 ml (rats) or 20 ml (mice) of fresh 4% paraformaldehyde (PFA, pH 7.4; Fisher Scientific, Hampton NH). Brains were rapidly removed, post-fixed in 4% PFA for 24 hr, and then transferred to 0.1M PBS containing 0.2% sodium azide (w/v) and stored at 4°C until sectioning. One hundred-micrometer thick coronal sections containing the PL cortex

(Rat coordinates: AP 2.76–4.2 mm from bregma, Mouse coordinates: AP 1.5–2 mm from bregma) and the NAc (Rat coordinates: AP 1.8–0.7 mm from bregma, Mouse coordinates: AP 1–1.4 mm from bregma) were sliced on a vibrating microtome (Leica Biosystems, VT1000 S). Serial sections were stored in 0.1M PBS with 0.2% sodium azide until processing. Three to four sections containing the PL cortex or the NAc were processed for immunohistochemical fluorescent detection of Iba1 or multiplex detection of Iba1 and GFP. Sections were blocked in 0.1M PBS containing 2% Triton X-100 (PBST) and 2% normal goat serum (NGS, Jackson Immunoresearch, # 005–000-121) for 2 hr at room temperature with agitation. This was followed by incubation in PBST containing 2% NGS and rab bit anti-Iba1 (1:1,000, Wako #019–19741, RRID:AB_839504) and chicken anti-GFP (1:1,000, Abcam, Cambridge UK, #ab13970, RRID:AB_300798) primary antisera overnight at 4°C with agitation. Additional details about each primary antibody can be found in Table 1. Sections were then washed 3 × 10 min in PBST, incubated in PBST containing 2% NGS with goat anti-chicken secondary antisera conjugated to Alexa Fluor® 488 (1:1,000, Abcam, Cambridge UK, #ab150169, RRID:AB_2636803) and/or goat anti-rabbit Alexa Fluor® 647 (1:1,000, Abcam, Cambridge UK, #ab150079, RRID: AB_2722623) for 5 hr at room temperature, washed 3 × 10 min in PBST, and then mounted on superfrost-plus slides with ProLong™ Gold Antifade (Invitrogen, Carlsbad CA, #P36930). Mounted slides were stored at 4°C until confocal imaging.

2.5 | Confocal microscopy

All imaging and analyses were performed by an investigator blind to experimental groups. Confocal *Z*-series image data sets of Iba1+ microglia were captured using a Leica SP8 laser-scanning confo cal microscope with a 63X (N.A. 1.4) oil-immersion objective. The parameters for imaging acquisition involved two separate modalities. The first set of parameters was designed to image networks of microglia for high-throughput analyses of the somatic dimensions. These high-throughput data sets were acquired using a diode 638 nm laser line, 2,048 × 2,048 frame size, 0.75X digital zoom, and a *Z*-step size of 0.37 μm. The entirety of all visible Iba1 signal was collected throughout the thickness of the slice (data sets spanning 70–100 μm). The second set of imaging parameters, which were optimized for examining individual microglial cells at high resolution, involved image acquisition using the same objective and laser line, 2,336 × 2,336 frame size, 1.5X digital zoom, and a *Z*-step size of 0.24 μm. Data sets collected with this modality typically spanned 50–70 μm. For the high-resolution single-cell imaging approach, care was taken to ensure that the entirety of the cell was collected in the image by positioning the soma in the middle of the *Z*-stack during imaging. This ensured that all microglial processes for the cell of interest, projecting radially and axially, were completely collected. Microglia in the PL cortex were imaged in layer V while those in the NAc were imaged in the core (NAcore) region dorsomedial to the anterior commissure.

2.6 | Imaris 3D reconstruction and analysis

Following confocal image acquisition, *Z*-series data sets were imported into Imaris software (Version 9.0, Bitplane, Belfast, UK). For high-throughput analyses of somatic dimensions, a smooth 3D space-filling model was constructed in order to best fit microglial cell bodies in a semi-automated manner. Inaccurate or falsely recognized somas were adjusted or removed,

respectively, by an investigator blind to experimental groups. The total number of cells contained within a field, as well as each microglial soma volume, were exported.

Confocal data sets containing high-resolution *Z*-stacks of individual microglia were imported to Imaris for 3D modeling, skeletonization, branching, and Sholl analyses. Three to six cells were imaged per animal for Air and CIE-exposed rats, and five to eight cells were imaged per animal for LPS-exposed rats. Once an individual microglial cell with its reconstructed fine processes was isolated, the Filament module in Imaris was used to skeletonize each microglia in a semi-automated process. For this procedure, the thinnest process diameter was set to 0.5 μm and the overall seed size diameter was set to 8 μm. Each microglia skeletonization was then visually inspected and manually adjusted to best fit the Iba1 signal with care. Next, the filament module was combined with a MATLAB plugin to produce a 3D convex hull for each cell. This shape is mathematically defined as the minimum polyhedron that can contain the filament resulting from skeletonization. This convex hull was used as an index of the 3D territory that each microglia occupied. Skeletonization analyses of the microglial processes included determination of 3D Sholl intersections obtained as a function of distance from the cells center (the middle of the soma), measurement of the convex hull volume (in μm^3) as an index of territory occupied, the overall cellular volume of microglia (soma and processes), and determination of the number of filament branch points.

For comparison of Iba1 immunohistochemical detection with the detection of immunoamplified EYFP in Cx3cr1 transgenic mice, 24 cells were imaged and isolated as described above. In this case, Iba1 was used as the source channel for isolating individual cells, then a 3D space-filling model was built on both Iba1 and EYFP. The overall volume of each cell for each source channel was then compared. Three to four sections were imaged per animal.

2.7 | Statistical analyses

Sample sizes were chosen based on the previous findings regarding CIE-induced adaptations in electrophysiological properties in prefrontal cortical neurons (Trantham-Davidson et al., 2014). Statistical analyses were performed using GraphPad Prism software (version 6, GraphPad, San Diego, CA). Normality of data was analyzed using Shapiro-Wilk test. If data within a group were found to be non-normally distributed, a corrected analysis was performed as specified in the results. Withdrawal scores were analyzed with a Geisser-Greenhouse-corrected repeated measures one-way ANOVA followed by Dunnett's multiple comparison test comparing days 10 and 15 to day 5. When three groups were compared across a single dependent variable, a one-way ANOVA was used. Tukey's multiple comparison test was used when a significant effect of treatment (LPS or CIE vs. control) was revealed. The number of Sholl intersections as a function of distance from soma start point was analyzed with a two-way repeated measures ANOVA with treatment (CIE or LPS vs. Naïve) as a between-subjects variable and distance from soma center as a within-subjects variable. Bonferroni-corrected pairwise comparison test was used when a significant interaction was observed. For high-throughput analyses, the average soma volume was calculated for each confocal data set collected; values were generated for four to six data

sets per animal. These values were then used to generate an animal average, then animal averages were reported. Individual soma volume for each animal in each group were also plotted as independent data points to investigate population shifts in microglia soma volume as a function of treatment and analyzed with three individual Kolomogorov-Smirnov tests comparing control to CIE, control to LPS, and CIE to LPS. A paired student's *t*-test was used when comparing the cell volume of Iba1 compared to cell volume of Cx3cr1-EYFP. Data are expressed as the mean ± *SD* and significance was set at $p < 0.05$.

3 | RESULTS

In the present study, we examined microglial morphology in the PL cortex and NAc of brain sections obtained from three experimental groups of rats: an ethanol-naïve control group, a group of rats that had been subjected to CIE and sacrificed 10 hr following the last ethanol exposure, and a group of rats that had been injected with LPS once daily for two consecutive days and then sacrificed 24 hr later (Figure 1).

3.1 | Iba1 labeling of microglia compared to transgenic mice

Iba1 immunoreactivity has canonically been used to classify microglia morphological profiles (Shapiro, Perez, Foresti, Arisi, & Ribak, 2009). However, isolation and labeling of microglia with genetic labeling approaches, including transgenic mice expressing YFP under direction of the Cx3cr1 promoter, has been used previously as a means for morphological analyses (Gu et al., 2016; Lehmann, Cooper, Maric, & Herkenham, 2016). To our knowledge, a direct comparison between the efficacy of labeling microglia with genetically encoded reporter compared to Iba1 immunohistochemistry has yet to be performed. Accordingly, we first performed a control experiment to demonstrate the fidelity of Iba1 immunohistochemistry as a means to fully label microglia syncytia in both the PL cortex and the NAc. Figure 2a,b shows Iba1 immunohistochemical detection (red) and EYFP (green) from Cx3cr1 transgenic mice in the PL cortex. Three to four images of microglia were sampled per animal. Figure 2c,d shows the same immunohistochemical detection in the NAc and Figure 2e,f shows a higher magnification merge. As shown in Figure 2g, a two-tailed paired *t*-test indicated that the cell volume (in μm^3) derived from the EYFP source channel (1708 ± 452.8) was slightly lower than that of the Iba1 source channel (1934 ± 639.1) in the PL cortex ($t(9) = 2.28$, $p = 0.049$). As shown in Figure 2h, the EYFP source channel (1,466 ± 463.8) was also significantly lower than that of the Iba1 source channel (1804 ± 414.3) in the NAc ($t(7) = 4.67$, $p = 0.002$). Thus, Iba1 immunohistochemistry produced a slightly more complete labeling of microglial cells than that was obtained following EYFP immunohistochemistry in both the PL cortex and the NAcore of Cx3cr1 transgenic mice.

4 | Measurements of blood ethanol concentration, withdrawal scores, and representative immunohistochemical detection of Iba1 in the PL cortex and NAcore

To obtain quantitative measures of alcohol intoxication and physical dependence, intoxication and withdrawal scoring were performed daily while BECs were obtained on four separate days of CIE exposure from tail-vein blood. As shown in Figure S1a, the BEC

averaged across all 4 days was 294.4 ± 76.19. The corresponding level of intoxication averaged across all days was 2.17 ± 0.385 (Figure S1b), which equates to a mild-to-moderate level of intoxication based upon the parameters of the rating scale. A Geisser-Greenhouse-corrected repeated measures one-way ANOVA comparing withdrawal scores across time revealed a significant effect of time ($F_{(1.8, 7.2)} = 17.00$, $p = 0.002$, Figure S1c). Dunnett's multiple comparison test indicated that rats on both day 10 ($p = 0.034$) and day 15 ($p = 0.012$) exhibited significantly higher withdrawal scores compared to day 5.

Studies demonstrate that CIE induces adaptations in the PL cortex that drive dysfunctional cognitive processing (Trantham-Davidson et al., 2014), and disruptions in cognition have been linked to altered microglia activation profiles (for review see Blank & Prinz, 2013). In addition, the NAcore undergoes CIE-induced adaptations that drive excessive drinking, which have also been linked to the increased expression of genes linked to the inflammatory reponse (Osterndorff-Kahanek et al., 2015). Accordingly, immunohistochemical labeling and subsequent confocal imaging of Iba1+ microglia were carried out in sections containing these regions. Figure 3a shows the region sampled in the PL cortex and Figure 3b shows a representative low magnification immunohistochemical detection of Iba1 in the PL cortex, whereas Figure 3c shows a representative higher magnification image of several Iba1+ microglia. Figure 3d shows the representative region sampled in the NAcore and Figure 3e,f shows low and high magnification images of Iba1 detection in the NAcore.

4.1 | High throughput, population-based analyses on microglia density and soma volume in the PL cortex and NAcore after CIE or LPS exposure

In the PL cortex, Iba1 immunostaining produced robust labeling of microglia in sections obtained from control (Figure 4a, $n = 5$), CIE-exposed (Figure 4b, $n = 5$), and LPS injected rats (Figure 4c, $n = 5$). Dimensions of the somatic compartment of microglia cells were analyzed using 3D space-filling models, which were color coded to indicate somatic volume in μm^3. We imaged four to six fields of microglia in the PL cortex for each rat, and generated data for five rats for each condition, resulting in a total of 958 cells in the control group, 951 cells in CIE-exposed animals, and 902 cells in LPS-exposed animals. When these data were collapsed and expressed as an average across all rats in a group, a one-way ANOVA revealed a significant main effect of treatment on the number of cells/μm^3 ($F_{(2, 12)} = 5.25$, $p = 0.023$). Tukey's multiple comparison test indicated that CIE ($p = 0.024$), but not LPS ($p = 0.791$) exposure decreased the number of cells/μm^3 when compared to control rats (Figure 4d). In addition, a significant main effect of treatment was also observed for somatic volume ($F_{(2, 12)} = 20.61$, $p = 0.0001$; Figure 4e). Post hoc analysis with Tukey's multiple comparison tests indicated that while CIE did not significantly increase microglia soma volume relative to control rats ($p = 0.263$), LPS-treated rats exhibited a robust increase in soma volume relative to control ($p = 0.0001$) and CIE-exposed rats ($p = 0.002$). As shown in Figure S2a, we also generated cumulative frequency distributions of soma volume that presents each cell imaged and quantified as an individual data point, akin to the approach that was previously used to analyze population shifts in dendritic spine morphology (Radley et al., 2015; Siemsen, Giannotti, McFaddin, Scofield, & McGinty, 2018). Comparison of the microglial soma volume cumulative frequency distribution in the PL cortex of CIE-exposed rats to the cumulative frequency distribution in control rats revealed a significant rightward

shift in the somatic volume distribution (K-S $D = 0.13$, $p < 0.0001$). The fact that this difference was not present in the animal averages reflects the subtlety of CIE's impact on soma volume. As expected, cumulative frequency distributions of LPS-exposed rats show a pronounced rightward shift in the soma volume distribution when compared to control animals (K-S $D = 0.31$, $p < 0.0001$) and to CIE-exposed rats (K-S $D = 0.20$, $p < 0.0001$).

Immunostaining for Iba1 in the NAcore also produced robust signal across all groups (Figure 5a–c). As with the PL cortex, we imaged four to six fields of microglia for each animal, and imaged a total of five animals. This produced a total of 929 total cells in control rats, 833 total cells in CIE-exposed rats, and 942 total cells in LPS-exposed rats. Analysis of the immunostaining in the NAcore of the three experimental groups of rats yielded a significant main effect of treatment on the number of cells per μm^3 when collapsed across animals ($F_{(2, 12)} = 6.72$, $p = 0.011$). Tukey's multiple comparison test further indicated that LPS ($p = 0.009$), but not CIE ($p = 0.295$), exposure reduced the number of cells per μm^3, when compared to control rats (Figure 5d), an effect that was opposite to that observed in the PL cortex. There was also a significant main effect of treatment on the average soma volume ($F_{(2, 12)} = 17.43$, $p = 0.0003$). Tukey's multiple comparison test indicated that LPS exposure resulted in a significant increase in microglia soma volume when compared to control rats ($p = 0.0004$) and CIE-exposed rats ($p = 0.001$, Figure 5e). As described above for the PL cortex, each cell from each group was also expressed as an individual data point that resulted in a cumulative frequency distribution of soma volume (Figure S2b). As was the case with the PL cortex, comparison of CIE-exposed rats to control rats revealed a subtle rightward shift in the somatic volume distribution in the NAcore (K-S $D = 0.09$, $p < 0.01$). LPS exposure was again associated with a more dramatic rightward shift in the somatic volume frequency distribution of microglia in the NAcore compared to control (K-S $D = 0.32$, $p < 0.0001$) and CIE-exposed rats (K-S $D = 0.24$, $p < 0.0001$).

Finally, when comparing cells/μm^3 and soma volume between brain regions and across treatments, a two-way repeated measures ANOVA revealed a significant treatment by brain region interaction for cells/μm^3 ($F_{(2, 12)} = 7.34$, $p = 0.008$, Figure S3a). Bonferroni-corrected pairwise comparison test indicated that control animals showed a larger amount of microglia normalized to the data set volume in the NAcore compared to PL cortex ($p = 0.02$) as did CIE-treated animals ($p = 0.004$). A two-way repeated measures ANOVA also revealed a significant main effect of brain region for soma volume ($F_{(2, 12)} = 71.60$, $p < 0.0001$, Figure S3b), yet there was no significant treatment by brain region interaction ($F_{(2, 12)} = 0.986$, $p = 0.40$), indicating that microglia soma volume is greater in the PL cortex compared to the NAcore in general.

4.2 | Dichotomous changes in microglial morphology and complexity following CIE and LPS exposure in the PL cortex and NAcore revealed by high-resolution single-cell imaging

To quantify and assess microglial structure reorganization following CIE or LPS exposure, we used high-resolution microscopy with imaging parameters designed to fully capture individual microglia and their corresponding process fields. As shown in the representative images in Figure 6a–c, Iba1 immunohistochemical detection revealed detailed microglial cells in the PL cortex. Once the imaged cell was digitally isolated and skeletonized in 3D,

assessment of the complexity of microglial arbors using Sholl sphere analysis was carried out (radii set at 1 μm intervals from the center of the cell). A two-way repeated measures ANOVA revealed a significant treatment by distance interaction for LPS compared to control rats ($F_{(49, 392)} = 3.981$, $p < 0.0001$; Figure 6d). Further, Bonferroni-corrected pairwise comparison tests indicated that LPS-treated rats had a significantly greater number of Sholl sphere breaks at 11–14 μm from the center of the cell ($p < 0.05$). However, there was no significant treatment by distance interaction of the number of intersections for CIE-exposed versus control rats ($F_{(49, 392)} = 1.16$, $p = 0.216$).

Isolated individual microglia in the PL cortex were digitally rendered, using space-filling models, to determine microglia cell volume. At the single-cell level, space-filling models were generated for the entire microglial cell, including both the soma and processes. As is shown in Figure 6e, a one-way ANOVA revealed a significant main effect of treatment on cell volume ($F_{(2, 12)} = 22$, $p < 0.0001$). Tukey's multiple comparison test further revealed that microglia of CIE-exposed rats had significantly lower overall cellular volume compared to the control group ($p = 0.03$). In contrast, LPS-exposed rats exhibited significantly larger overall cellular volume compared to controls ($p = 0.008$) and CIE-exposed rats ($p < 0.0001$). The intensity of Iba1 signal within the somatic compartment was quantified and expressed relative to the whole cell intensity. A one-way ANOVA revealed a significant main effect of treatment ($F_{(2, 12)} = 28.58$, $p < 0.0001$, Figure 6f). Tukey's multiple comparison test indicated that CIE ($p = 0.026$) and LPS ($p < 0.0001$)-treated rats displayed increased normalized Iba1 intensity compared to controls, whereas LPS displayed a significantly greater Iba1 intensity increase when compared to CIE ($p = 0.002$). Polygonal convex hulls generated from skeletonized microglial processes were then used to assess the spatial territory individual cells occupy. This index has been commonly used as a means to normalize the measures of morphological complexity (Morrison et al., 2017). A one-way ANOVA revealed that there was no difference between groups in the average cellular territory (convex hull) that individual PL cortex microglia occupy within the parenchyma ($F_{(2, 12)} = 0.55$, $p = 0.589$, Figure 6g). Another parameter used to describe microglia structure and complexity is the degree and extent of process branching. As shown in Figure 6h, a one-way ANOVA comparing the number of branch points relative to convex hull volume also revealed a main effect of treatment ($F_{(2, 12)} = 29.02$, $p < 0.0001$). Tukey's multiple comparison test revealed that CIE exposure reduced branch points ($p = 0.007$), whereas LPS increased the number of branch points when compared to both control ($p = 0.006$) and CIE-exposed rats ($p < 0.0001$). As a final measure of cellular complexity, the total number of Sholl intersections was expressed relative to convex hull volume. A one-way ANOVA revealed a significant main effect of treatment ($F_{(2, 12)} = 10.53$, $p = 0.002$), with Tukey's multiple comparison test indicating that neither CIE ($p = 0.127$) nor LPS ($p = 0.072$) exposure significantly decreased the number of Sholl intersections when normalized to the hull volume compared to control rats. However, LPS exposure increased the number of Sholl intersections when compared to CIE rats ($p = 0.002$, Figure 6i).

The single-cell structural analysis approach was next used to assess the morphological properties of microglia in the NAcore. Representative confocal images of the microglia in the NAcore for the three experimental groups are presented in Figure 7a–c. As was observed with microglia in the PL cortex, a two-way repeated measures ANOVA revealed a

significant treatment by distance interaction in the number of Sholl intersections in LPS-exposed rats compared to control rats ($F_{(49, 392)} = 8.78$, $p < 0.0001$ Figure 7d). Bonferroni-corrected pairwise comparison tests indicated that LPS exposure significantly increased the number of Sholl intersections at 11–14 and 16–23 microns from the center of the cell ($p < 0.05$). Although there was a significant treatment by distance interaction in the number of Sholl intersections in CIE compared to control rats ($F_{(49, 392)} = 1.49$, $p = 0.022$), Bonferroni-corrected pairwise comparison tests indicated there were no significant differences between CIE and control. A one-way ANOVA comparing microglial cell volume between the three groups indicated a significant main effect of treatment ($F_{(2, 12)} = 5.21$, $p = 0.024$, Figure 7e). However, Tukey's multiple comparison test indicated a significant difference between CIEand LPS-exposed rats ($p = 0.019$), but no significant difference for either CIE ($p = 0.341$) or LPS ($p = 0.225$) compared to controls. As described above, we quantified the intensity of the Iba1 signal within the somatic compartment and expressed this as relative whole cell intensity. A one-way ANOVA revealed a significant main effect of treatment ($F_{(2, 12)} = 8.88$, $p = 0.004$, Figure 7f). Tukey's multiple comparison test indicated that LPS increased the normalized Iba1 intensity compared to control rats ($p = 0.004$), yet there was no significant difference between control and CIE-exposed rats ($p = 0.307$). Analysis of the convex hull volume in the NAcore revealed that data from control animals were non-normally distributed (W = 0.630, $p = 0.001$). A Kruskal-Wallis nonparametric one-way ANOVA revealed there were no significant group differences in the extent of territory covered by microglial processes (K-W = 3.62, $p = 0.171$, Figure 7g). A one-way ANOVA revealed no significant effect of treatment on the number of branch points normalized to convex hull volume ($F_{(2, 12)} = 1.55$, $p = 0.253$, Figure 7h), and the number of Sholl intersections normalized to convex hull volume was also not significantly different between groups ($F_{(2, 12)} = 2.77$, $p = 0.102$, Figure 7i).

5 | DISCUSSION

The results of the current study revealed that CIE and LPS exposure differentially alter the morphological profile of microglia, as revealed by immunohistochemical detection of Iba1, 3D digital reconstruction of confocal images, and analysis of morphometric properties. A summary of these findings can be found in Table 2 and are discussed in detail below. Our study revealed basal differences in microglia density in the PL cortex compared to NAcore, with the NAcore showing greater density of microglia in the control and CIE-, but not LPS-treated rats. This finding is in general agreement with an early study showing increased microglia density in the mouse striatum relative to the frontal cortex (Lawson, Perry, Dri, & Gordon, 1990) as well a study showing increased Iba1 immunoreactive material in the NAcore compared to PL cortex (Tynan et al., 2010). This was coincident with a general reduction in microglia soma volume in the NAcore compared to PL cortex. Rats that were rendered dependent on ethanol by 15 days of CIE exposure and sacrificed 10 hr into withdrawal exhibited brain region-dependent alterations in morphologic properties of microglia that were distinct from those induced by LPS in both the PL cortex and NAcore, two relevant nodes of the addiction and cognitive neurocircuitry (Chaudhri, Sahuque, Cone, & Janak, 2008; George et al., 2012). When fields of microglia in the PL cortex were sampled in rats exposed to LPS, we observed an increase in microglial somatic volume

compared to controls and CIE-exposed rats. Consistent with what others have shown for alcohol (Sanchez-Alavez et al., 2019) and LPS (Bodea et al., 2014) exposure, high magnification confocal imaging of individual microglia demonstrated that both CIE and LPS exposure increased Iba1 intensity within the somatic compartment, an effect consistent with microglial activation (Hovens, Nyakas, & Schoemaker, 2014). Interestingly, CIE-, but not LPS-mediated increases in somatic Iba1 intensity were specific to the PL cortex. LPS exposure significantly increased various indices of PL cortical microglial complexity (overall cell volume, branch points/μm^3 territory), yet PL microglia from CIE-exposed rats exhibited reductions in these same indices. Further, we observed that morphological alterations in the NAcore due to both LPS and CIE exposure were of substantially lower magnitude when compared to the PL cortex, indicating the observed effects are brain region dependent. This is likely not due to basal differences in the ability of Iba1 to fully label microglia in these two brain regions given that comparisons of Cx3cr1-EYFP and Iba1 labeling in both the PL cortex and NAcore produced nearly identical results, with Iba1 actually producing slightly more complete labeling. Taken together, these data suggest that CIE and LPS produce dichotomous alterations in microglial process architecture in which CIE simplified and LPS increased microglia process branching. These distinct morphometric signatures may reflect unique aspects of the correspondingly distinct pathophysiologies engaged by CIE and withdrawal, relative to LPS exposure. Moreover, these findings suggest that careful analyses of microglia architecture using a single-cell imaging approach can reveal discrete alterations in microglia morphological complexity that could be overlooked with more coarse analyses of parameters like soma size and Iba1 intensity.

5.1 | LPS has heterogenous effects on somatic volume and complexity

LPS binds to and activates several receptors on innate immune cells and the most well-characterized are CD14, TLR2, and TLR4 (Fenton & Golenbock, 1998). TLR2 responds to gram-positive bacteria whereas TLR4 responds to gram-negative bacteria (Takeuchi et al., 1999). Moreover, injection of mice with peptides interfering with TLR4 prevents LPS-induced secondary messenger cascades, cytokine release, microglia structural reorganization, as well as associated sickness behavior (Hines et al., 2013). Thus, the most likely candidate for engaging microglia reorganization in our studies is TLR4, although the contribution of these other receptors to LPS-induced microglia reorganization in our studies cannot be excluded. Although it is well-documented that LPS exposure activates microglia by binding to TLR4 and engaging the innate immune response, ultimately driving increased cytokine release, the degree to which LPS engages alterations in microglia morphometric properties is highly dependent on the dose and timeframe. Consistent with our data, LPS exposure at doses similar to that was used in the present study produced a hyper-ramified morphological profile characterized by an increased soma size and increased branching (Hinwood et al., 2013; Morrison et al., 2017). Activated microglia that display the hyper-ramified structural profile have also been observed following chronic stress (Hellwig et al., 2016), ischemic stroke (Morrison & Filosa, 2013), and traumatic brain injury (Morrison et al., 2017). In addition, we show that LPS-induced increases in soma size occurring in the PL cortex are also associated with increased overall cell volume in conjunction with the increased branching complexity and number of branch points.

Our data are largely consistent with a previous study showing that 24 hr after exposure to a low-dose LPS microglia soma volume is increased in the mPFC with no alteration in the number of cells (Kongsui, Johnson, Graham, Nilsson, & Walker, 2015). Also consistent with our results, this study demonstrated that LPS increased process thickness and branching complexity (Kongsui et al., 2015). However, our data provide new evidence that LPS-mediated increases in soma volume are brain region-independent, whereas increases in branching patterns were largely brain region-dependent given that they were not observed in the NAcore. Taken together, these findings indicate that enlarged soma volume and enhanced Iba1 intensity coincide with heightened microglia activation. However, the brain region-specificity revealed by our data suggest that branching patterns are likely a more nuanced metric that may reflect unique aspects of a specific activation profile. Taken together, our data indicate that LPS has a greater impact on PL cortical microglia morphology compared to microglia in the NAcore. Given that the PL cortex regulates multiple cognitive processes (Granon & Poucet, 2000), and that frontal cortical-dependent processing of emotionally relevant stimuli is disrupted following LPS administration in humans (Kullmann et al., 2013), this finding suggests that the PL cortex-specific alterations in microglial complexity following LPS may play a role in the cognitive decline following exposure to environmental insults such as traumatic brain injury.

5.2 | CIE-induced alterations in microglia branching complexity occur in a brain region-dependent manner

At a global level, the frontal cortex and NAc exhibit anatomically unique gene expression profiles in humans with AUD (Mayfield et al., 2002), including genes linked to the induction of neuroinflammatory responses (Flatscher-Bader et al., 2006). Specifically, within the subset of alcohol-responsive genes, only 6% are shared between the frontal cortex and NAc (Flatscher-Bader et al., 2005). Consistent with this human data, CIE in rodents alters the expression level of a larger amount of alcohol-responsive genes in the PL cortex when compared to the NAcore (Melendez, McGinty, Kalivas, & Becker, 2012). The data presented here are also consistent with the hypothesis that the microglia in the PL cortex are more responsive to CIE when compared to microglia in the NAcore. We demonstrate that simplifications in microglia process density during withdrawal from CIE, a microglial morphological signature commonly observed in aged rodents (Udeochu, Shea, & Villeda, 2016), occur in the PL cortex and not in the NAcore. Thus, the greater impact of alcohol exposure on gene expression in the cortex may contribute to the brain region-specificity of the effects on microglial cellular architecture described in our study. However, whether these brain region-specific morphological differences translate to functionally differential characteristics of microglial activation remain to be fully determined. Given that microglia play an important role in shaping synaptic plasticity by releasing neuroimmune modulators (Wake, Moorhouse, Jinno, Kohsaka, & Nabekura, 2009), our data are consistent with the suggestion that microglial-mediated neural circuit adaptation following chronic ethanol exposure and withdrawal could be mechanistically distinct in the PL cortex when compared to the NAcore.

5.3 | Comparing withdrawal from CIE- and LPS-mediated microglial activation

Microglial activation has been implicated in the regulation of the neural processes linked to cognition, memory, and associative learning, as well as with the neuroplasticity and neuropathology associated with acute and chronic exposure to alcohol (Blank & Prinz, 2013; Chastain & Sarkar, 2014; Fernandez-Lizarbe et al., 2009; Henriques et al., 2018; Kohman, 2012; Kyrargyri, Vega-Flores, Gruart, Delgado-García, & Probert, 2015). While it is clear that LPS-induced activation of microglia via TLR4 leads to an induction of the pro-inflammatory cytokine TNFα, the ability of ethanol exposure to do the same is currently under debate (Bi et al., 2005; Fernandez-Lizarbe et al., 2009). As an example, prolonged (6 months) ethanol exposure increased the overall proportion of activated microglia relative to total microglia in the hippocampus, yet did not impact TNFα expression (Cruz et al., 2017). Furthermore, binge-like alcohol exposure during adolescence increased CD11b immunoreactivity in the hippocampus, an additional measure of microglial activation (Zhao et al., 2013), yet did not alter TNFα expression (Marshall et al., 2013). This differential impact of ethanol and LPS on microglia TNFα expression may explain dichotomous impacts of ethanol exposure and LPS exposure on overall microglia volume or branching patterns.

An emerging concept that is gaining support is that ethanol exposure produces a state of “partial activation” of microglia (Marshall et al., 2013; Yang et al., 2014). Given that LPS increased both somatic Iba1 intensity and soma volume to a greater extent than CIE, our data support this hypothesis. However, at the single-cell level, we observed that microglia display two disparate and unique morphological signatures following CIE and withdrawal or LPS exposure. While we observed a decreased number of microglia, reduced overall cell volume, and decreased branching following CIE, there was an increase in overall cell volume and process density following exposure to LPS but no alteration in the total number of microglia. Of particular interest, the differential change in total microglia density in the PL cortex following CIE treatment could be due to cell death, lack of proliferation, or a combination. Microglia density remains stable over adulthood due to coupled proliferation and apoptosis (Askew et al., 2017) and such a balance is disrupted in human alcoholics given that human alcoholics display decreased numbers of glia in the prefrontal cortex (Miguel-Hidalgo et al., 2002). Our findings generally agree with a previous study showing that adolescent ethanol exposure decreases the number of glia in the PL cortex in adulthood, without affecting the number of neurons, though this study did not differentiate microglia from astroglia (Koss, Sadowski, Sherrill, Gulley, & Juraska, 2012). Interestingly, this effect was specific to male rats, which is also the sex that was utilized in the present study. Accordingly, one caveat of our study is that we did not study female rats. There may indeed be potential sex differences in microglia morphometric features in the PL cortex of CIE-exposed rats, and this should be an avenue of future investigation. Regardless, our data suggest that the decreased number of PL cortical microglia in CIE-exposed rats could confer a state of hyporesponsiveness to immune challenges. Thus, an alternative hypothesis is that CIE leads to hypoactivation of microglia in the PL cortex. In our data set, reduced process density and overall cell volume could serve as evidence for hypoactivation. This interpretation would suggest that following chronic alcohol exposure, microglia in the PL cortex may be less responsive to activation and thus less suited to fulfill their protective role following additional environmental insults

(Kreutzberg, 1996). This may be reflected as reduced ability to release cytokines, decreased overall microglial process mobility, and disrupted phagocytosis (Frank et al., 2006). This conclusion is supported by prior findings indicating that ethanol inhibits the ability of microglia to induce phagocytosis of opsonized *Escherichia coli* in culture (Aroor & Baker, 1998).

As described above, we observed reduced microglia cell volume and branching following CIE exposure in the PL cortex. This represents a structural profile similar to that has been observed in the neocortex of Alzheimer's patients (Davies, Ma, Jegathees, & Goldsbury, 2017) and in rodent models of aging (Norden & Godbout, 2013; Udeochu et al., 2016). In contrast, after two 1 mg/kg systemic administrations of LPS separated by 24 hr, we observed increased microglia cell volume and branching. These dichotomous morphological signatures could also be consistent with another unique hypothesis, whereby LPSand CIE-mediated microglial activation produce mechanistically distinct gene expression and cytokine and chemokine release patterns. Consistent with this hypothesis, binge alcohol exposure during adolescence leads to increased microglia proliferation during adulthood, independent of phagocytic activity or increased MHC-II expression commonly associated with "activated" microglia (McClain, Morris, et al., 2011). Thus, ethanol-induced microglia activation is likely independent of the innate immune reaction observed in microglia following LPS treatment (i.e., upregulation of MHC-II) (Buttini, Limonta, & Boddeke, 1996). Additional experimentation is required to determine if CIE and withdrawal produces partial activation, hypoactivation, or a mechanistically unique activation state in PL cortical microglia. However, in light of the ongoing revisions to the cellular, molecular, and structural characteristics associated with microglia activation states (Ransohoff, 2016), the use of high-resolution microscopy and digital reconstruction will no doubt provide new structural biomarkers that can be used to better understand how alterations in cellular complexity relate to microglial function.

Remodeling of microglia architecture is thought to be a pre-requisite for the ability of microglia to respond to changes in the local environment by releasing cytokines and other neuromodulators. Further, altered Iba1 expression is a major component of this structural reorganization (Walker et al., 2014). A well-established means for microglia to alter synaptic communication is through the phagocytosis of synaptic elements, termed "synaptic stripping" (Kettenmann et al., 2013). Interestingly, more recent reports indicate that this occurs through a process termed "trogocytosis" that involves partial phagocytosis of presynaptic axon boutons as opposed to postsynaptic dendritic spines (Weinhard et al., 2018). Although we did not experimentally determine whether altered microglia morphometric features in CIE and LPS-exposed rats resulted in functional reorganization of neuronal structure and function, some inferences can be made regarding this effect based on the our data. Reduced microglial structural complexity in the PL cortex of CIE-exposed rats could confer an inability of microglia to extend processes toward synapses and regulate the synaptic strength at these synapses through physical engulfment. This would fit nicely with the hypothesis described above whereby microglia are in a hypoactive state in the PL cortex during withdrawal from CIE. Given that CIE increases the prevalence of mushroom type spines on layer V mPFC basal dendrites (Kroener et al., 2012) and increases the NMDA component of excitatory postsynaptic currents (Kroener et al., 2012) and evoked NMDA

amplitude (Trantham-Davidson et al., 2014), it is conceivable that this could be due to an inability of microglia to properly regulate synaptic strength, potentiating discrete inputs onto layer V PL cortical pyramidal neurons. However, our findings may not support this as we observed that LPS increased the complexity of microglia in the PL cortex. In contrast to CIE, LPS treatment using a similar dosing paradigm leads to a long-term, but delayed, decrease in dendritic spine density in the neocortex due to destabilization of preexisting spines (Kondo, Kohsaka, & Okabe, 2011). This could be interpreted as a homeostatic response to increased neuronal activity given that TNFα released from microglia acts as a potent regulator of synaptic scaling (Stellwagen & Malenka, 2006). Increased microglia complexity in LPS-treated rats could, therefore, confer a state of hyper trogocytosis, ultimately degrading entire synapses. Future experiments should focus on determining the structural and functional consequence of altered microglia complexity revealed herein.

6 | CONCLUSION

LPS had a profound impact on soma volume in both the PL cortex and NAcore when compared to CIE. However, CIE exposure reduced multiple indices of microglia complexity whereas LPS increased such measurements, an effect that was relegated to the PL cortex. Interestingly, our examination of microglial morphological profiles at high magnification revealed that CIE exposure produced a structural profile that is similar to what has been reported in Alzheimer's disease (Davies et al., 2017) and in rodent models of aging (Norden & Godbout, 2013; Udeochu et al., 2016). In contrast, LPS produced a structural profile that is more similar to what has been observed following chronic stress (Hellwig et al., 2016), ischemic stroke (Morrison & Filosa, 2013), and traumatic brain injury (Morrison et al., 2017). The present study may lay a framework for high fidelity imaging and 3D structural characterization following distinct environmental insults, and that usage of the methods described herein will allow for a better understanding of the scope of microglial diversity through high structural characterization and classification.

Supplementary Material

Refer to Web version on PubMed Central for supplementary material.

ACKNOWLEDCMENTS

The authors thank Dr. Christopher Cowan and Catherine Bridges for providing *Cx3cr1*^{CreER}-EYFP transgenic mice.

Funding information

National Institute on Drug Abuse, Grant/Award Number: R00 DA040004 and T32 DA007288; National Institute on Alcohol Abuse and Alcoholism, Grant/Award Number: R01 AA010983 and R01 AA022701

REFERENCES

Agrawal RG, Hewetson A, George CM, Syapin PJ, & Bergeson S (2011). Minocycline reduces ethanol drinking. Brain, Behavior, and Immunity, 25(Suppl. 1), S165–S169. 10.1016/j.bbi.2011.03.002

Ahmed Z, Shaw G, Sharma VP, Yang C, McGowan E, & Dickson DW (2007). Actin-binding proteins coronin-1a and IBA-1 are effective microglial markers for immunohistochemistry. Journal of

Histochemistry and Cytochemistry, 55(7), 687–700. 10.1369/jhc.6A7156.2007 [PubMed: 17341475]

Alfonso-Loeches S, Pascual-Lucas M, Blanco AM, Sanchez-Vera I, & Guerri C (2010). Pivotal role of TLR4 receptors in alcohol-induced neuroinflammation and brain damage. Journal of Neuroscience, 30(24), 8285–8295. 10.1523/JNEUROSCI.0976-10.2010 [PubMed: 20554880]

Aroor AR, & Baker RC (1998). Ethanol inhibition of phagocytosis and superoxide anion production by microglia. Alcohol, 15(4), 277–280. 10.1016/S0741-8329(97)00129-8 [PubMed: 9590511]

Askew K, Li K, Olmos-Alonso A, Garcia-Moreno F, Liang Y, Richardson P, … Gomez-Nicola D (2017). Coupled proliferation and apoptosis maintain the rapid turnover of microglia in the adult brain. Cell Reports, 18(2), 391–405. 10.1016/j.celrep.2016.12.041 [PubMed: 28076784]

Avignone E, Lepleux M, Angibaud J, & Nägerl UV (2015). Altered morphological dynamics of activated microglia after induction of status epilepticus. Journal of Neuroinflammation, 12, 202. [PubMed: 26538404]

Beech RD, Qu J, Leffert JJ, Lin A, Hong KA, Hansen J, … Sinha R (2012). Altered expression of cytokine signaling pathway genes in peripheral blood cells of alcohol dependent subjects: Preliminary findings. Alcoholism, Clinical and Experimental Research, 36(9), 1487–1496. 10.1111/j.1530-0277.2012.01775.x

Beynon SB, & Walker FR (2012). Microglial activation in the injured and healthy brain: What are we really talking about? Practical and theoretical issues associated with the measurement of changes in microglial morphology. Neuroscience, 225, 162–171. 10.1016/j.neuroscience.2012.07.029 [PubMed: 22824429]

Bi XL, Yang JY, Dong YX, Wang JM, Cui YH, & Ikeshima T, … Wu CF (2005). Resveratrol inhibits nitric oxide and TNF-alpha production by lipopolysaccharide-activated microglia. International Immunopharmacology, 5(1), 185–193. [PubMed: 15589480]

Blank T, & Prinz M (2013). Microglia as modulators of cognition and neuropsychiatric disorders. Glia, 61(1), 62–70. 10.1002/glia.22372 [PubMed: 22740320]

Bodea LG, Wang Y, Linnartz-Gerlach B, Kopatz J, Sinkkonen L, Musgrove R, … Neumann H (2014). Neurodegeneration by activation of the microglial complement-phagosome pathway. Journal of Neuroscience, 34(25), 8546–8556. 10.1523/JNEUROSCI.5002-13.2014 [PubMed: 24948809]

Bohatschek M, Kloss CUA, Kalla R, & Raivich G (2001). In vitro model of microglial deramification: Ramified microglia transform into amoeboid phagocytes following addition of brain cell membranes to microglia-astrocyte cocultures. Journal of Neuroscience Research, 64(5), 508–522. [PubMed: 11391706]

Bult CJ, Blake JA, Smith CL, Kadin JA, Richardson JE, Anagnostopoulos A, … Zhu Y (2018). Mouse genome database (MGD) 2019. Nucleic Acids Research, 47(D1), D801–D806. 10.1093/nar/gky1056

Buttini M, Limonta S, & Boddeke HW (1996). Peripheral administration of lipopolysaccharide induces activation of microglial cells in rat brain. Neurochemistry International, 29(1), 25–35. [PubMed: 8808786]

Chastain LG, & Sarkar DK (2014). Role of microglia in regulation of ethanol neurotoxic action. International Review of Neurobiology, 118, 81–103. [PubMed: 25175862]

Chaudhri N, Sahuque LL, Cone JJ, & Janak PH (2008). Reinstated ethanol-seeking in rats is modulated by environmental context and requires the nucleus accumbens core. European Journal of Neuroscience, 28(11), 2288–2298. 10.1111/j.1460-9568.2008.06517.x

Crews FT, Walter TJ, Coleman LG, & Vetreno RP (2017). Toll-like receptor signaling and stages of addiction. Psychopharmacology, 234(9–10), 1483–1498. 10.1007/s00213-017-4560-6 [PubMed: 28210782]

Crews FT, & Vetreno RP (2016). Mechanisms of neuroimmune gene induction in alcoholism. Psychopharmacology, 233(9), 1543–1557. 10.1007/s00213-015-3906-1 [PubMed: 25787746]

Cruz C, Meireles M, & Silva SM (2017). Chronic ethanol intake induces partial microglial activation that is not reversed by long-term ethanol withdrawal in the rat hippocampal formation. Neurotoxicology, 60, 107–115. 10.1016/j.neuro.2017.04.005 [PubMed: 28408342]

Czeh M, Gressens P, & Kaindl AM (2011). The yin and yang of microglia. Developmental Neuroscience, 33(3–4), 199–209. 10.1159/000328989 [PubMed: 21757877]

Davies DS, Ma J, Jegathees T, & Goldsbury C (2017). Microglia show altered morphology and reduced arborization in human brain during aging and Alzheimer's disease. Brain Pathology, 27(6), 795–808. 10.1111/bpa.12456 [PubMed: 27862631]

Davis BM, Salinas-Navarro M, Cordeiro MF, Moons L, & De Groef L (2017). Characterizing microglia activation: A spatial statistics approach to maximize information extraction. Scientific Reports, 7(1), 1576. 10.1038/s41598-017-01747-8 [PubMed: 28484229]

Devalaraja MN, Mcclain CJ, Barve S, Vaddi K, & Hill DB (1999). Increased monocyte MCP-1 production in acute alcoholic hepatitis. Cytokine, 11(11), 875–881. 10.1006/cyto.1999.0495 [PubMed: 10547276]

Dubbelaar ML, Kracht L, Eggen BJ, & Boddeke EW (2018). The kaleidoscope of microglial phenotypes. Frontiers in Immunology, 9, 1753. [PubMed: 30108586]

Fenton MJ, & Golenbock DT (1998). LPS-binding proteins and receptors. Journal of Leukocyte Biology, 64(1), 25–32. 10.1002/jlb.64.1.25 [PubMed: 9665271]

Fernández-Arjona MDM, Grondona JM, Granados-Durán P, Fernández-Llebrez P, & López-Ávalos MD (2017). Microglia morphological categorization in a rat model of neuroinflammation by hierarchical cluster and principal components analysis. Frontiers in Cellular Neuroscience, 11, 235. [PubMed: 28848398]

Fernandez-Lizarbe S, Pascual M, & Guerri C (2009). Critical role of TLR4 response in the activation of microglia induced by ethanol. Journal of Immunology, 183(7), 4733–4744. 10.4049/jimmunol.0803590

Flatscher-Bader T, van der Brug M, Hwang JW, Gochee PA, Matsumoto I, Niwa SI, & Wilce PA (2005). Alcohol-responsive genes in the frontal cortex and nucleus accumbens of human alcoholics. Journal of Neurochemistry, 93(2), 359–370. 10.1111/j.1471-4159.2004.03021.x [PubMed: 15816859]

Flatscher-Bader T, van der Brug MP, Landis N, Hwang JW, Harrison E, & Wilce PA (2006). Comparative gene expression in brain regions of human alcoholics. Genes, Brain, and Behavior, 5(Suppl. 1), 78–84. 10.1111/j.1601-183X.2006.00197.x

Frank MG, Barrientos RM, Biedenkapp JC, Rudy JW, Watkins LR, & Maier SF (2006). mRNA up-regulation of MHC II and pivotal pro-inflammatory genes in normal brain aging. Neurobiology of Aging, 27(5), 717–722. 10.1016/j.neurobiolaging.2005.03.013 [PubMed: 15890435]

Gass JT, Glen WB, McGonigal JT, Trantham-Davidson H, Lopez MF, Randall PK, … Chandler LJ (2014). Adolescent alcohol exposure reduces behavioral flexibility, promotes disinhibition, and increases resistance to extinction of ethanol self-administration in adulthood. Neuropsychopharmacology, 39(11), 2570–2583. 10.1038/npp.2014.109 [PubMed: 24820536]

George O, Sanders C, Freiling J, Grigoryan E, Vu S, Allen CD, … Koob GF (2012). Recruitment of medial prefrontal cortex neurons during alcohol withdrawal predicts cognitive impairment and excessive alcohol drinking. Proceedings of the National Academy of Sciences of the United States of America, 109(44), 18156–18161. 10.1073/pnas.1116523109 [PubMed: 23071333]

Gilpin NW, Richardson HN, Cole M, & Koob GF (2008). Vapor inhalation of alcohol in rats. Current Protocols in Neuroscience, 44(1), 9–29.

Grabert K, Michoel T, Karavolos MH, Clohisey S, Baillie JK, Stevens MP, … McColl BW (2016). Microglial brain region-dependent diversity and selective regional sensitivities to aging. Nature Neuroscience, 19(3), 504–516. 10.1038/nn.4222 [PubMed: 26780511]

Granon S, & Poucet B (2000). Involvement of the rat prefrontal cortex in cognitive functions: A central role for the prelimbic area. Psychobiology, 28(2), 229–237.

Gu N, Eyo UB, Murugan M, Peng J, Matta S, Dong H, & Wu LJ (2016). Microglial P2Y12 receptors regulate microglial activation and surveillance during neuropathic pain. Brain, Behavior, and Immunity, 55, 82–92. 10.1016/j.bbi.2015.11.007

Harry GJ, & Kraft AD (2012). Microglia in the developing brain: A potential target with lifetime effects. Neurotoxicology, 33(2), 191–206. 10.1016/j.neuro.2012.01.012 [PubMed: 22322212]

He J, & Crews FT (2008). Increased MCP-1 and microglia in various regions of the human alcoholic brain. Experimental Neurology, 210(2), 349–358. 10.1016/j.expneurol.2007.11.017 [PubMed: 18190912]

Hellwig S, Brioschi S, Dieni S, Frings L, Masuch A, Blank T, & Biber K (2016). Altered microglia morphology and higher resilience to stress-induced depression-like behavior in CX3CR1-deficient mice. Brain, Behavior, and Immunity, 55, 126–137. 10.1016/j.bbi.2015.11.008

Henriques JF, Portugal CC, Canedo T, Relvas JB, Summavielle T, & Socodato R (2018). Microglia and alcohol meet at the crossroads: Microglia as critical modulators of alcohol neurotoxicity. Toxicology Letters, 283, 21–31. 10.1016/j.toxlet.2017.11.002 [PubMed: 29129797]

Hines DJ, Choi HB, Hines RM, Phillips AG, & MacVicar BA (2013). Prevention of LPS-induced microglia activation, cytokine production and sickness behavior with TLR4 receptor interfering peptides. PLoS One, 8(3), e60388. 10.1371/journal.pone.0060388 [PubMed: 23555964]

Hinwood M, Tynan RJ, Charnley J. l., Beynon SB, Day TA, & Walker FR (2013). Chronic stress induced remodeling of the prefrontal cortex: Structural re-organization of microglia and the inhibitory effect of minocycline. Cerebral Cortex, 23(8), 1784–1797. 10.1093/cercor/bhs151 [PubMed: 22710611]

Hovens I, Nyakas C, & Schoemaker R (2014). A novel method for evaluating microglial activation using ionized calcium-bind ing adaptor protein-1 staining: Cell body to cell size ratio. Neuroimmunology and Neuroinflammation, 1(2), 82. 10.4103/2347-8659.139719

Hutchinson MR, Northcutt AL, Hiranita T, Wang X, Lewis SS, Thomas J, … Watkins LR (2012). Opioid activation of toll-like receptor 4 contributes to drug reinforcement. Journal of Neuroscience, 32(33), 11187–11200. 10.1523/JNEUROSCI.0684-12.2012 [PubMed: 22895704]

Ito D, Imai Y, Ohsawa K, Nakajima K, Fukuuchi Y, & Kohsaka S (1998). Microglia-specific localisation of a novel calcium binding protein, Iba1. Molecular Brain Research, 57(1), 1–9. 10.1016/S0169-328X(98)00040-0 [PubMed: 9630473]

Karperien A, Ahammer H, & Jelinek HF (2013). Quantitating the subtleties of microglial morphology with fractal analysis. Frontiers in Cellular Neuroscience, 7, 3. [PubMed: 23386810]

Kettenmann H, Kirchhoff F, & Verkhratsky A (2013). Microglia: New roles for the synaptic stripper. Neuron, 77(1), 10–18. 10.1016/j.neuron.2012.12.023 [PubMed: 23312512]

Kigerl KA, de Rivero Vaccari JP, Dietrich WD, Popovich PG, & Keane RW (2014). Pattern recognition receptors and central nervous system repair. Experimental Neurology, 258, 5–16. 10.1016/j.expneurol.2014.01.001 [PubMed: 25017883]

Kohman RA (2012). Aging microglia: Relevance to cognition and neural plasticity. Methods in Molecular Biology, 934, 193–218. [PubMed: 22933148]

Kondo S, Kohsaka S, & Okabe S (2011). Long-term changes of spine dynamics and microglia after transient peripheral immune response triggered by LPS in vivo. Molecular Brain, 4, 27. [PubMed: 21682853]

Kongsui R, Johnson SJ, Graham BA, Nilsson M, & Walker FR (2015). A combined cumulative threshold spectra and digital reconstruction analysis reveal structural alterations of microglia within the prefrontal cortex following low-dose LPS administration. Neuroscience, 310, 629–640. 10.1016/j.neuroscience.2015.09.061 [PubMed: 26440295]

Koss WA, Sadowski RN, Sherrill LK, Gulley JM, & Juraska JM (2012). Effects of ethanol during adolescence on the number of neurons and glia in the medial prefrontal cortex and basolateral amygdala of adult male and female rats. Brain Research, 1466, 24–32. 10.1016/j.brainres.2012.05.023 [PubMed: 22627163]

Kranzler HR, & Soyka M (2018). Diagnosis and pharmacotherapy of alcohol use disorder: A review. JAMA, 320(8), 815–824. 10.1001/jama.2018.11406 [PubMed: 30167705]

Kreutzberg GW (1996). Microglia: A sensor for pathological events in the CNS. Trends in Neurosciences, 19(8), 312–318. 10.1016/0166-2236(96)10049-7 [PubMed: 8843599]

Kroener S, Mulholland PJ, New NN, Gass JT, Becker HC, & Chandler LJ (2012). Chronic alcohol exposure alters behavioral and synaptic plasticity of the rodent prefrontal cortex. PLoS One, 7(5), e37541. 10.1371/journal.pone.0037541 [PubMed: 22666364]

Kullmann JS, Grigoleit J-S, Lichte P, Kobbe P, Rosenberger C, Banner C, … Schedlowski M (2013). Neural response to emotional stimuli during experimental human endotoxemia. Human Brain Mapping, 34(9), 2217–2227. 10.1002/hbm.22063 [PubMed: 22461242]

Kyrargyri V, Vega-Flores G, Gruart A, Delgado-García JM, & Probert L (2015). Differential contributions of microglial and neuronal IKKbeta to synaptic plasticity and associative learning in alert behaving mice. Glia, 63(4), 549–566. [PubMed: 25297800]

Lawson LJ, Perry VH, Dri P, & Gordon S (1990). Heterogeneity in the distribution and morphology of microglia in the normal adult mouse brain. Neuroscience, 39(1), 151–170. 10.1016/0306-4522(90)90229-W [PubMed: 2089275]

Lehmann ML, Cooper HA, Maric D, & Herkenham M (2016). Social defeat induces depressive-like states and microglial activation without involvement of peripheral macrophages. Journal of Neuroinflammation, 13(1), 224. 10.1186/s12974-016-0672-x [PubMed: 27581371]

Liu D, Wang Z, Liu S, Wang F, Zhao S, & Hao A (2011). Antiinflammatory effects of fluoxetine in lipopolysaccharide(LPS)-stimulated microglial cells. Neuropharmacology, 61(4), 592–599. 10.1016/j.neuropharm.2011.04.033 [PubMed: 21575647]

Manzardo A, Poje A, Penick E, & Butler M (2016). Multiplex immunoassay of plasma cytokine levels in men with alcoholism and the relationship to psychiatric assessments. International Journal of Molecular Sciences, 17(4), 472. 10.3390/ijms17040472 [PubMed: 27043532]

Marshall SA, McClain JA, Kelso ML, Hopkins DM, Pauly JR, & Nixon K (2013). Microglial activation is not equivalent to neuroinflammation in alcohol-induced neurodegeneration: The importance of microglia phenotype. Neurobiology of Diseases, 54, 239–251. 10.1016/j.nbd.2012.12.016

Mayfield RD, Lewohl JM, Dodd PR, Herlihy A, Liu J, & Harris RA (2002). Patterns of gene expression are altered in the frontal and motor cortices of human alcoholics. Journal of Neurochemistry, 81(4), 802–813. 10.1046/j.1471-4159.2002.00860.x [PubMed: 12065639]

McClain JA, Hayes DM, Morris SA, & Nixon K (2011). Adolescent binge alcohol exposure alters hippocampal progenitor cell proliferation in rats: Effects on cell cycle kinetics. Journal of Comparative Neurology, 519(13), 2697–2710. 10.1002/cne.22647

McClain JA, Morris SA, Deeny MA, Marshall SA, Hayes DM, Kiser ZM, & Nixon K (2011). Adolescent binge alcohol exposure induces long-lasting partial activation of microglia. Brain, Behavior, and Immunity, 25(Suppl. 1), S120–S128. 10.1016/j.bbi.2011.01.006

Melendez RI, McGinty JF, Kalivas PW, & Becker HC (2012). Brain region-specific gene expression changes after chronic intermittent ethanol exposure and early withdrawal in C57BL/6J mice. Addiction Biology, 17(2), 351–364. 10.1111/j.1369-1600.2011.00357.x [PubMed: 21812870]

Miguel-Hidalgo JJ, Wei J, Andrew M, Overholser JC, Jurjus G, Stockmeier CA, & Rajkowska G (2002). Glia pathology in the prefrontal cortex in alcohol dependence with and without depressive symptoms. Biological Psychiatry, 52(12), 1121–1133. 10.1016/S0006-3223(02)01439-7 [PubMed: 12488057]

Morrison H, Young K, Qureshi M, Rowe RK, & Lifshitz J (2017). Quantitative microglia analyses reveal diverse morphologic responses in the rat cortex after diffuse brain injury. Scientific Reports, 7(1), 13211. 10.1038/s41598-017-13581-z [PubMed: 29038483]

Morrison HW, & Filosa JA (2013). A quantitative spatiotemporal analysis of microglia morphology during ischemic stroke and reperfusion. Journal of Neuroinflammation, 10, 4. [PubMed: 23311642]

Nimmerjahn A, Kirchhoff F, & Helmchen F (2005). Resting microglial cells are highly dynamic surveillants of brain parenchyma in vivo. Science, 308(5726), 1314–1318. 10.1126/science.1110647 [PubMed: 15831717]

Nixon K, & Crews FT (2002). Binge ethanol exposure decreases neurogenesis in adult rat hippocampus. Journal of Neurochemistry, 83(5), 1087–1093. 10.1046/j.1471-4159.2002.01214.x [PubMed: 12437579]

Norden DM, & Godbout JP (2013). Review: Microglia of the aged brain: Primed to be activated and resistant to regulation. Neuropathology and Applied Neurobiology, 39(1), 19–34. 10.1111/j.1365-2990.2012.01306.x [PubMed: 23039106]

Northcutt AL, Hutchinson MR, Wang X, Baratta MV, Hiranita T, Cochran TA, … Watkins LR (2015). DAT isn't all that: Cocaine reward and reinforcement require Toll-like receptor 4 signaling. Molecular Psychiatry, 20(12), 1525–1537. 10.1038/mp.2014.177 [PubMed: 25644383]

O'Dell LE, Roberts AJ, Smith RT, & Koob GF (2004). Enhanced alcohol self-administration after intermittent versus continuous alcohol vapor exposure. Alcoholism, Clinical and Experimental Research, 28(11), 1676–1682. 10.1097/01.ALC.0000145781.11923.4E

Olah M, Biber K, Vinet J, & Wgm Boddeke H (2011). Microglia phenotype diversity. CNS & Neurological Disorders: Drug Targets, 10(1), 108–118.

Olson JK, & Miller SD (2004). Microglia initiate central nervous system innate and adaptive immune responses through multiple TLRs. Journal of Immunology, 173(6), 3916–3924. 10.4049/jimmunol.173.6.3916

Osterndorff-Kahanek EA, Becker HC, Lopez MF, Farris SP, Tiwari GR, Nunez YO, … Mayfield RD (2015). Chronic ethanol exposure produces timeand brain region-dependent changes in gene coexpression networks. PLoS One, 10(3), e0121522. 10.1371/journal.pone.0121522 [PubMed: 25803291]

Qin L, & Crews FT (2012). NADPH oxidase and reactive oxygen species contribute to alcohol-induced microglial activation and neurodegeneration. Journal of Neuroinflammation, 9, 5. [PubMed: 22240163]

Radley JJ, Anderson RM, Cosme CV, Glanz RM, Miller MC, Romig-Martin SA, & LaLumiere RT (2015). The contingency of cocaine administration accounts for structural and functional medial prefrontal deficits and increased adrenocortical activation. Journal of Neuroscience, 35(34), 11897–11910. 10.1523/JNEUROSCI.4961-14.2015 [PubMed: 26311772]

Ransohoff RM (2016). A polarizing question: Do M1 and M2 microglia exist? Nature Neuroscience, 19(8), 987–991. [PubMed: 27459405]

Salter MW, & Stevens B (2017). Microglia emerge as central players in brain disease. Nature Medicine, 23(9), 1018–1027. 10.1038/nm.4397

Sanchez-Alavez M, Nguyen W, Mori S, Wills DN, Otero D, Ehlers CL, & Conti B (2019). Time course of microglia activation and brain and blood cytokine/chemokine levels following chronic ethanol exposure and protracted withdrawal in rats. Alcohol, 76, 37–45. 10.1016/j.alcohol.2018.07.005 [PubMed: 30554034]

Sarlus H, & Heneka MT (2017). Microglia in Alzheimer's disease. Journal of Clinical Investigation, 127(9), 3240–3249. 10.1172/JCI90606

Shapiro LA, Perez ZD, Foresti ML, Arisi GM, & Ribak CE (2009). Morphological and ultrastructural features of Iba1-immunolabeled microglial cells in the hippocampal dentate gyrus. Brain Research, 1266, 29–36. 10.1016/j.brainres.2009.02.031 [PubMed: 19249294]

Siemsen BM, Giannotti G, McFaddin JA, Scofield MD, & McGinty JF (2018). Biphasic effect of abstinence duration following cocaine self-administration on spine morphology and plasticity-related proteins in prelimbic cortical neurons projecting to the nucleus accumbens core. Brain Structure and Function, 224(2), 741–758. 10.1007/s00429-018-1805-z [PubMed: 30498893]

Stellwagen D, & Malenka RC (2006). Synaptic scaling mediated by glial TNF-alpha. Nature, 440(7087), 1054–1059. [PubMed: 16547515]

Takeuchi O, Hoshino K, Kawai T, Sanjo H, Takada H, Ogawa T, … Akira S (1999). Differential roles of TLR2 and TLR4 in recognition of gram-negative and gram-positive bacterial cell wall components. Immunity, 11(4), 443–451. 10.1016/S1074-7613(00)80119-3 [PubMed: 10549626]

Trantham-Davidson H, Burnett EJ, Gass JT, Lopez MF, Mulholland PJ, Centanni SW, … Chandler L (2014). Chronic alcohol disrupts dopamine receptor activity and the cognitive function of the medial prefrontal cortex. Journal of Neuroscience, 34(10), 3706–3718. 10.1523/JNEUROSCI.0623-13.2014 [PubMed: 24599469]

Tsai G, & Coyle JT (1998). The role of glutamatergic neurotransmission in the pathophysiology of alcoholism. Annual Review of Medicine, 49, 173–184. 10.1146/annurev.med.49.1.173

Tynan RJ, Naicker S, Hinwood M, Nalivaiko E, Buller KM, Pow DV, … Walker FR (2010). Chronic stress alters the density and morphology of microglia in a subset of stress-responsive brain regions. Brain, Behavior, and Immunity, 24(7), 1058–1068. 10.1016/j.bbi.2010.02.001

Udeochu JC, Shea JM, & Villeda SA (2016). Microglia communication: Parallels between aging and Alzheimer's disease. Clinical and Experimental Neuroimmunology, 7(2), 114–125. 10.1111/cen3.12307 [PubMed: 27840659]

Wake H, Moorhouse AJ, Jinno S, Kohsaka S, & Nabekura J (2009). Resting microglia directly monitor the functional state of synapses in vivo and determine the fate of ischemic terminals. Journal of Neuroscience, 29(13), 3974–3980. 10.1523/JNEUROSCI.4363-08.2009 [PubMed: 19339593]

Walker FR, Beynon SB, Jones KA, Zhao Z, Kongsui R, Cairns M, & Nilsson M (2014). Dynamic structural remodelling of microglia in health and disease: A review of the models, the signals and the mechanisms. Brain, Behavior, and Immunity, 37, 1–14. 10.1016/j.bbi.2013.12.010

Weinhard L, di Bartolomei G, Bolasco G, Machado P, Schieber NL, Neniskyte U, … Schwab Y (2018). Microglia remodel synapses by presynaptic trogocytosis and spine head filopodia induction. Nature Communications, 9(1), 1228. 10.1038/s41467-018-03566-5

Wendeln AC, Degenhardt K, Kaurani L, Gertig M, Ulas T, & Jain G (2018). Innate immune memory in the brain shapes neurological disease hallmarks. Nature, 556(7701), 332–338. 10.1038/s41586-018-0023-4 [PubMed: 29643512]

Yang JY, Xue X, Tian H, Wang XX, Dong YX, Wang F, … Wu CF (2014). Role of microglia in ethanol-induced neurodegenerative disease: Pathological and behavioral dysfunction at different developmental stages. Pharmacology & Therapeutics, 144(3), 321–337. 10.1016/j.pharmthera.2014.07.002 [PubMed: 25017304]

Zhao YN, Wang F, Fan YX, Ping GF, Yang JY, & Wu CF (2013). Activated microglia are implicated in cognitive deficits, neuronal death, and successful recovery following intermittent ethanol exposure. Behavioral Brain Research, 236(1), 270–282. 10.1016/j.bbr.2012.08.052

Significance

Microglia-mediated neuroimmune activation normally provides protection of the central nervous system following environmental insults. Chronic ethanol exposure induces dysfunctional cognitive processes potentially linked to aberrant microglia activation. The data presented here demonstrate that both lipopolysaccharide (LPS) and chronic ethanol exposure lead to structural reorganization of microglia. However, we observed dichotomous ethanol- and LPS-mediated alterations in microglia morphometric features at the single-cell level. Further, ethanol-mediated effects were specific to the prelimbic cortex as opposed to the nucleus accumbens. Taken together, our findings suggest that ethanol-induced neurotoxicity may be independent of the innate immune response associated with microglia activation by LPS.

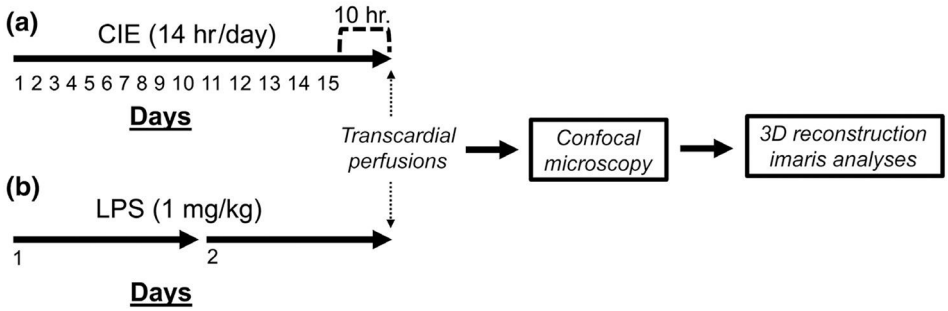

FIGURE 1.

Schematic depiction of the experimental timeline. (a) Timeline depicting the length of chronic intermittent ethanol (CIE) and the sacrifice time-point during withdrawal. (b) Timeline depicting the number of lipopolysaccharide (LPS) injections received and the sacrifice time-point following LPS exposure. CIE- or LPS-treated rats were compared to ethanol-naïve controls on each measure

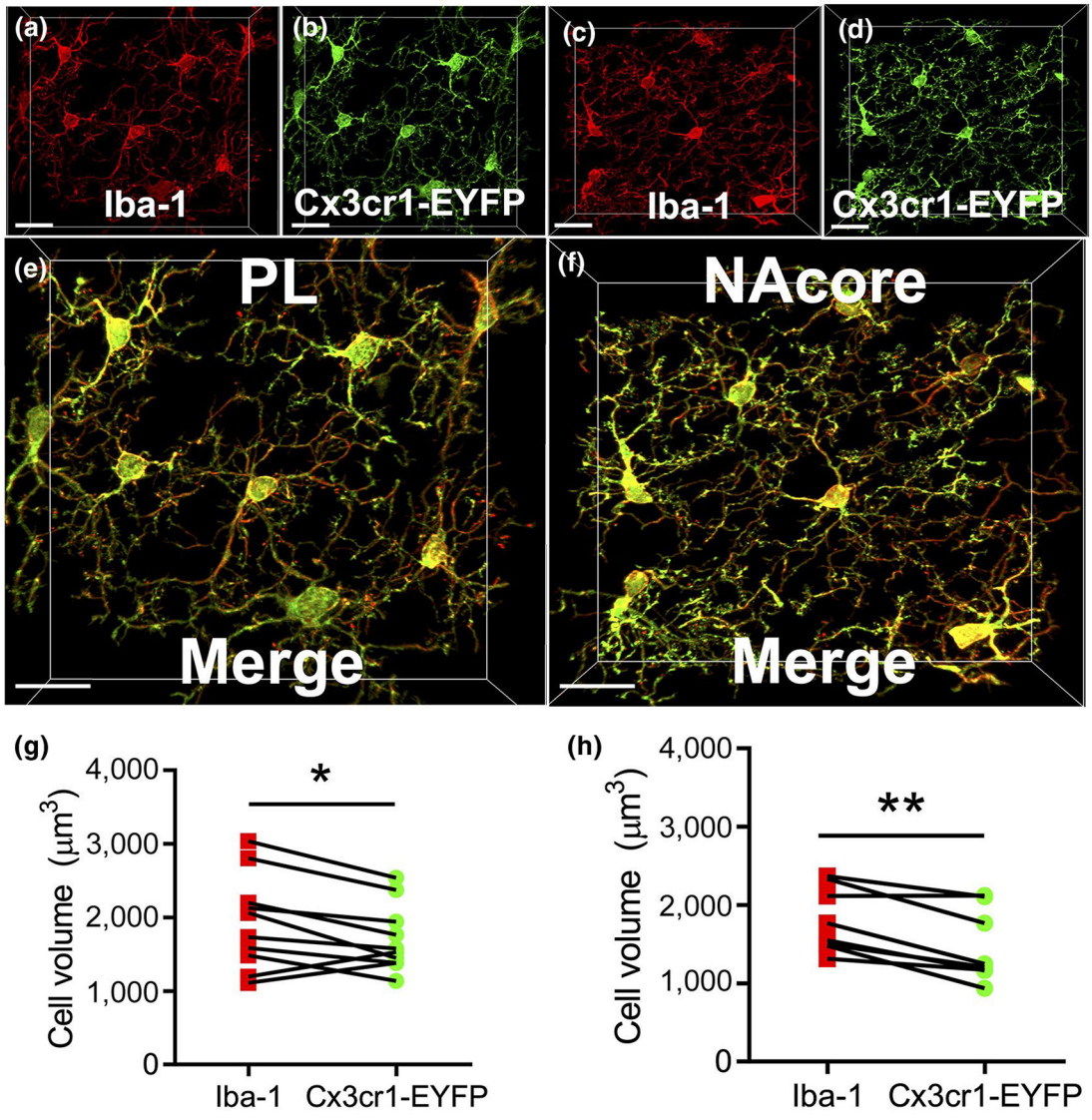

FIGURE 2.

Cellular reconstructions of microglia from genetic and immunofluorescent labeling techniques produce similar results. (a,b) Labeling produced by Iba1 IHC (Red) and Cx3cr1-EYFP fluorescence (Green) in the prelimbic (PL) portion of the PFC in Cx3cr1-EYFP mice ($n = 3$). Isolation of microglia for cell volume analyses were done as described within the materials and methods section. (c,d) Labeling produced by Iba1 IHC and Cx3cr1-EYFP fluorescence in the NAcore in Cx3cr1-EYFP mice. (e,f) High magnification merged image of data shown in (a-d). (g,h) Quantification of isolated cell volume using either Iba1 or Cx3cr1-EYFP signal as the source channel in PL cortex (g) and NAcore (h). Scale bars = 20 µm

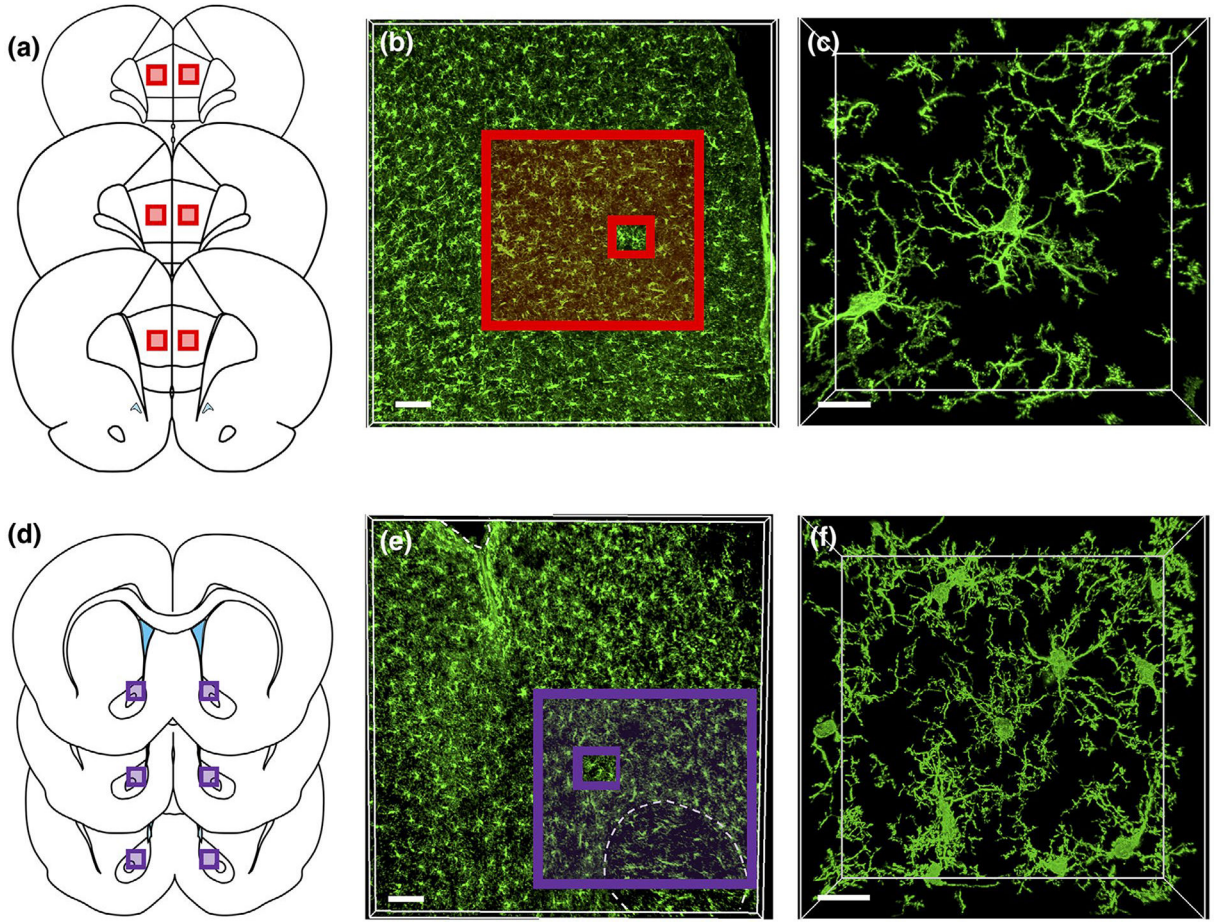

FIGURE 3.

Representative microglia syncytia in the prelimbic (PL) cortex and NAcore (a) The PL subdivision of the medial prefrontal cortex was sampled along the anterior-posterior axis. (b) Low-magnification image of Iba1 immunoreactivity in the PL cortex. (c) High-magnification image of Iba1 immunoreactive microglia in the PL cortex. The outer red-boxed region in (b) represents the area that corresponds to the box region shown in (a), while the smaller inset red box represents the image area shown in (c). (d) The NAcore subdivision of the nucleus accumbens was also sampled from sections across the anterior-posterior axis as described above. (b) Low-magnification images of Iba1 immunoreactivity in the NAcore. (c) Higher magnification image of Iba1 immunoreactive microglia in the NAcore. As above, the outer purple-boxed region in (e) represents the area that corresponds to the box region shown in (d) while the smaller inset purple box represents the image area shown in (f). Scale bars = 100 μm (b,e) and 15 μm (c,f)

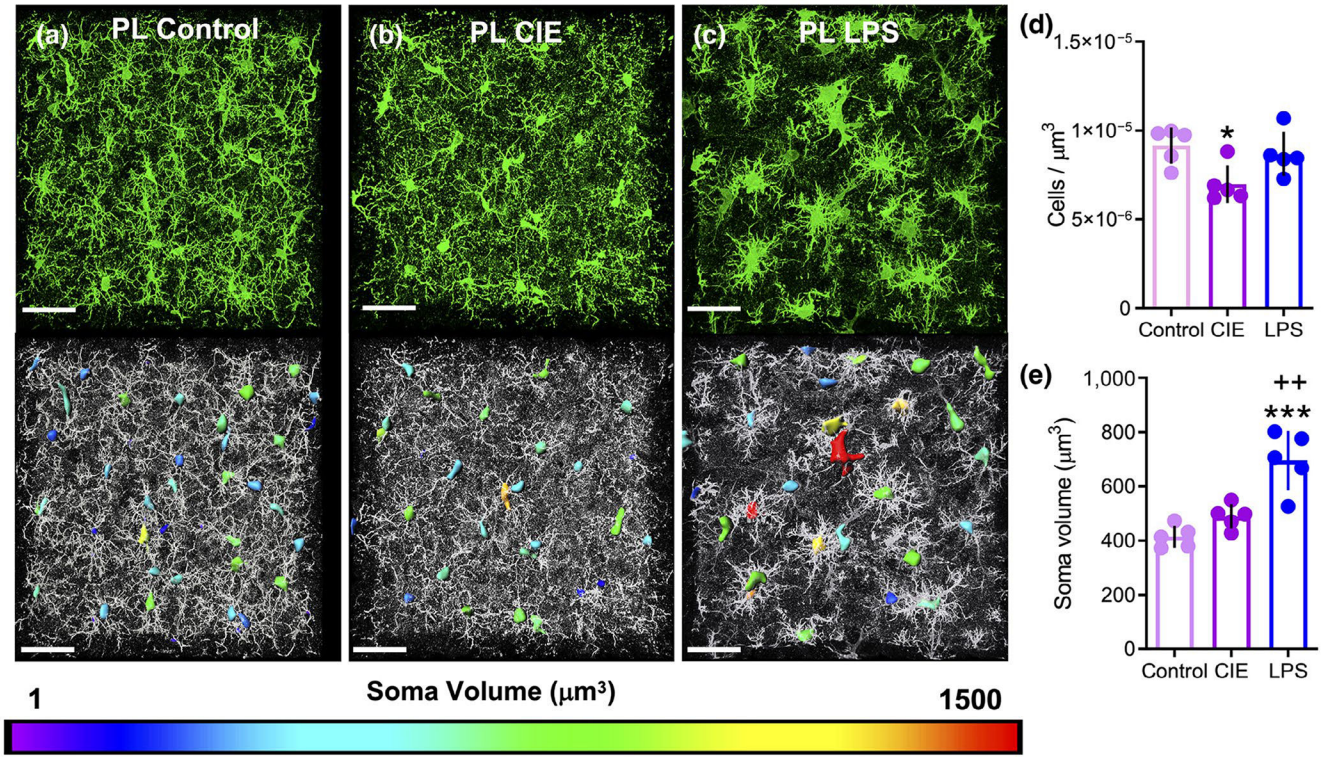

FIGURE 4.

Lipopolysaccharide (LPS), but not chronic intermittent ethanol (CIE), exposure resulted in an increase in somatic volume of microglia in the prelimbic (PL) cortex. Representative Iba1 staining of microglia in the PL cortex for control (a), CIE-exposed (b), and LPS-exposed (c) rats. Somas are color-coded to indicate the spectrum of soma volumes observed for each treatment. (d) CIE exposure reduced the number of Iba1 immunoreactive microglia per micron^3 in the PL cortex. (e) LPS (but not CIE) exposure was associated with a significant increase in the somatic volume when compared to control rats. *$p < 0.05$, ***$p < 0.001$ compared to control, ++$p < 0.01$ compared to CIE. Scale bar = 40 µm

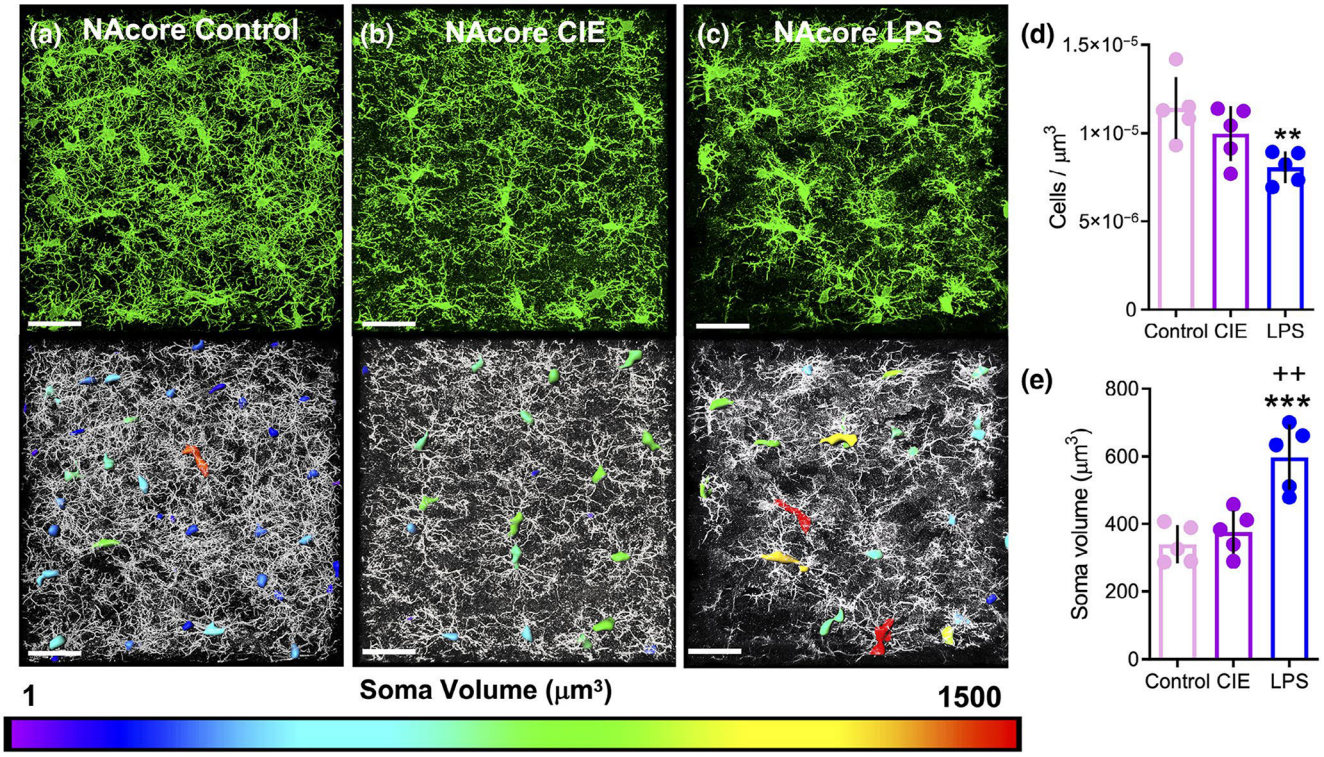

FIGURE 5.

Lipopolysaccharide (LPS), but not chronic intermittent ethanol (CIE), exposure resulted in an increase in somatic volume of microglia in the NAcore. (a) Representative Iba1 staining of microglia in the NAcore of control, (b) CIE, and (c) LPS-exposed rats. Somas are color-coded to indicate the spectrum of soma volumes observed for each treatment. (d) LPS-exposed rats exhibited a reduction in the number of Iba1 immunoreactive microglia per micron^3 in the NAcore. (e) When soma volume was averaged across all images for each animal, only LPS significantly increased the soma volume compared to control rats. *$p <$ 0.05, ***$p < 0.001$ compared to control, ++$p < 0.01$ compared to CIE. Scale bar = 40 µm

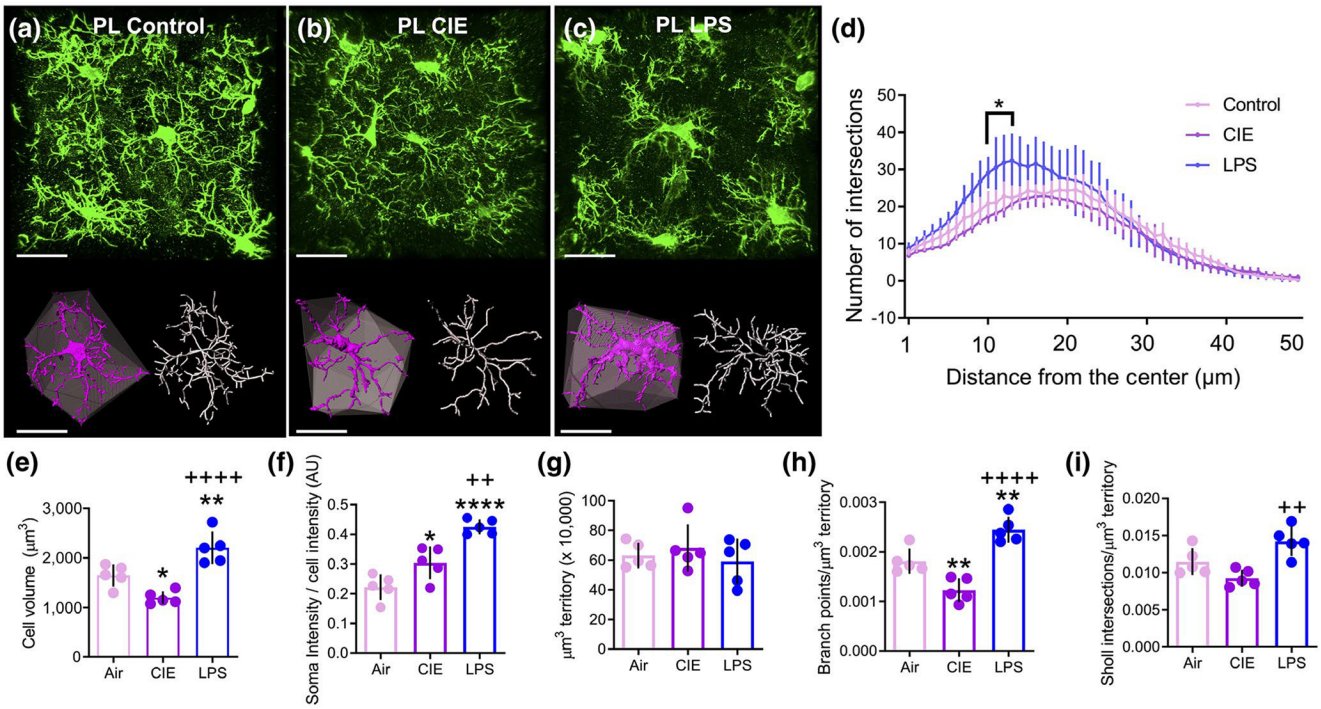

FIGURE 6.

Chronic intermittent ethanol (CIE) and lipopolysaccharide (LPS) exposure resulted in dichotomous alterations in microglia complexity in the prelimbic (PL) cortex. (a-c) Raw data (green), digitized single-cells (purple) and associated convex hulls (grey), as well as skeletonizations (white) for PL cortex microglia in (a) control, (b) CIE-exposed, and (c) LPS-exposed rats. (d) Sholl analysis revealed that LPS exposure resulted in a greater number of breaks (in 1 μm intervals) closer to the center of the cell compared to control rats. (e) CIE exposure reduced while LPS exposure increased the average volume of microglia. (f) CIE and LPS increased the normalized Iba1 intensity in the somatic compartment, with LPS producing a larger effect than CIE. (g) There was no difference between groups in the average territory occupied by microglia ("Hull" volume). (h) When normalized to the convex hull volume, CIE exposure decreased while LPS increased the number of branch points. (i) When normalized to the hull volume, there was no effect of CIE or LPS in the number of Sholl intersections compared to control rats in the PL cortex, yet LPS was significantly different compared to CIE. *$p < 0.05$, **$p < 0.01$, ****$p < 0.0001$ compared to control, ++$p < 0.01$, ++++ $p < 0.0001$ compared to CIE. Scale bars = 20 μm

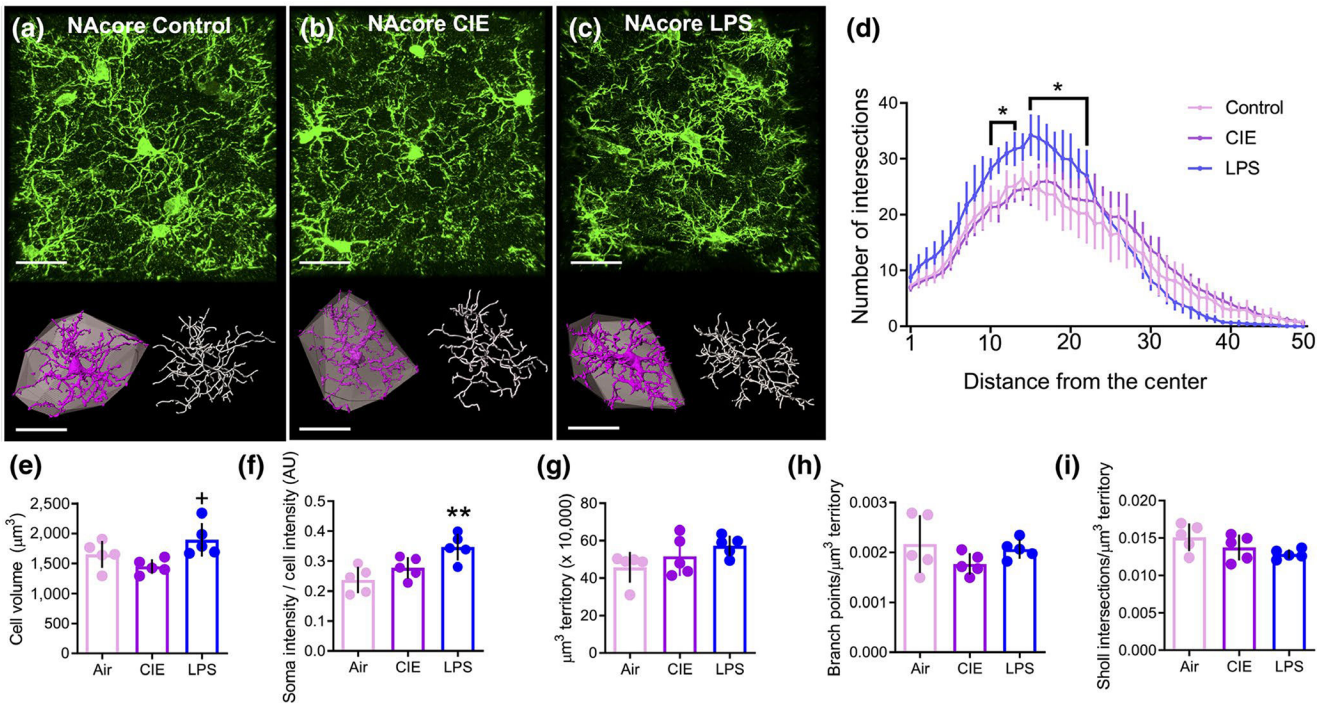

FIGURE 7.

Differential effects of chronic intermittent ethanol (CIE) and lipopolysaccharide (LPS) on microglial complexity were not observed in the NAcore. (a-c) Raw data (green), digitized single-cells (purple) and associated convex hulls (grey), as well as skeletonizations (white) for NAcore microglia in (a) control, (b) CIE-exposed, and (c) LPS-exposed rats. (d) Sholl analysis revealed that LPS exposure resulted in a greater number of breaks (in 1 µm intervals) closer to the center of the cell compared to control rats. (e) LPS increased the microglia cell volume compared to control, but CIE was without an effect. (f) LPS, but not CIE, increased the normalized Iba1 intensity in the somatic compartment. (g) There was no difference between groups in the territory occupied by individual microglia. (h) When normalized to the territory occupied, there was no difference between groups in the number of branch points. (i) The number of Sholl intersections normalized to the hull volume was not different between groups in the NAcore. $^{**}p < 0.01$ compared to control, $^{+}p < 0.05$ compared to CIE. Scale bars = 20 µm

TABLE 1

Table containing specific information about primary antisera used

Antibody	Immunogen Structure	Specific details	Concentration
Iba1	Synthetic peptide, C-terminal of Iba1	Wako chemicals #019-19741 RRID:AB_839504 Rabbit polyclonal	1:1,000
GFP	Recombinant full-length protein corresponding to GFP	Abcam #ab13970 RRID:AB_300798 Chicken polyclonal	1:1,000

TABLE 2

Table summarizing all microglial morphological changes in the PL and NAcore

Treatment	Brain region	Cells/μm^3	Soma volume	Cell volume	Normalized soma intensity	Territory occupied	Branch points	Sholl intersections
CIE	PL		–			–		–
LPS	PL	–				–		
CIE	NAcore	–	–	–	–	–	–	–
LPS	NAcore					–	–	–

Note: Solid black arrows indicate a change relative to control, and open arrows indicate a change relative to CIE. Horizontal lines indicate no difference compared to control.